A general method for structure prediction of metal-ligand interfaces of hybrid nanoparticles

Sami Malola[1], Paavo Nieminen[2], Antti Pihlajamäki[1], Joonas Hämäläinen[2], Tommi Kärkkäinen[2,*] and Hannu Häkkinen[1,3,*]

[1] Department of Physics, Nanoscience Center, University of Jyväskylä, FI-40014 Jyväskylä, Finland

[2] Faculty of Information Technology, University of Jyväskylä, FI-40014 Jyväskylä, Finland

[3] Department of Chemistry, Nanoscience Center, University of Jyväskylä, FI-40014 Jyväskylä, Finland

* email: tommi.karkkainen@jyu.fi ; hannu.j.hakkinen@jyu.fi

Abstract

Hybrid metal nanoparticles, consisting of a nano-crystalline metal core and a protecting shell of organic ligand molecules, have applications in diverse areas such as biolabeling, catalysis, nanomedicine, and solar energy. Despite a rapidly growing database of experimentally determined atom-precise nanoparticle structures and their properties, there has been no successful, systematic way to predict the atomistic structure of the metal-ligand interface. Here, we devise and validate a general method to predict the structure of the metal-ligand interface of ligand-stabilized gold and silver nanoparticles, based on information about local chemical environments of atoms in experimental data. In addition to predicting realistic interface structures, our method is useful for investigations on the steric effects at the metal-ligand interface, as well as for predicting isomers and intermediate structures induced by thermal dynamics or interactions with the environment. Our method is applicable to other hybrid nanomaterials once a suitable set of reference structures is available.

Hybrid metal nanoparticles, consisting of a nano-crystalline metal core and a protecting layer (shell) of organic ligand molecules, are an emerging class of functional nanomaterials that have potential applications in diverse areas such as biolabeling, catalysis, nanomedicine and solar energy. [1-8] The core-shell framework structure of hybrid nanoparticles offers ample opportunities to tune the physico-chemical properties and functionalities of the particles via controlling the size, shape, elemental composition, and structure of the metal core, together with the chemical composition of the ligand shell. The chemical interactions between the metal atoms and ligand molecules at the core-shell interface are in a crucial role since they dictate the atomic-scale structure, stability, and ensuing properties of the particle.

The last decade has witnessed clear advancements in synthesis and experimental structural characterization of very small, atomically precise hybrid nanoparticles with 1-3 nm cores made of metals, stabilized by various organic ligands.[3] These particles are also called monolayer-protected clusters, MPCs, and they represent an interesting subclass of nanoparticles since their structures can be often characterized to atomic precision by using X-ray diffraction method on single MPC crystals. At the moment, more than 150 crystallographically solved structures of MPCs, involving noble metals, main group metals, and various ligand molecules such as thiols, phosphines and alkynyls, have been reported. [3] This facilitates fundamental studies of the structure-property relationships both experimentally and computationally.

In most cases, however, the knowledge of the nanoparticle structures does not reach the atom-level resolution and the ligand-metal interfaces may be ill-defined. Only partial structural knowledge may be available, *e.g.*, by high-resolution electron microscopy where only the heavy atoms (metals) of the core may be visible.[9,10] Smallest particles may have low-symmetry or disordered metal cores, and may not be amenable at all to experimental techniques that work well for structural characterization of atomically ordered bulk materials.[11] A practical solution is then to reach conclusions of potential atomic-scale structures by comparing measured properties, such as powder X-ray diffraction data, and various spectroscopic data, to computed properties based on extensive sets of potential candidate structures. A crucial question is then how realistic is the group of the candidate structures, *i.e*, can the structure corresponding to the true global total energy minimum be included in that group with a high probability. In general, global optimization methods suffer from limitations arising from a prohibitively (exponentially) increasing number of local energy minima in the structural space for system sizes that

are larger than just a few metal atoms and ligand molecules. Another time-constraint arises from the fact that most measurable properties must be calculated numerically from the electronic structure using the platform of the density functional theory (DFT), which limits the number of structural candidates that can be examined. It is thus crucial to develop methods that can effectively suggest realistic atomic-scale structures at a very low computational cost.

The data on atomically precise structures of MPCs, combined with an ever-growing number measurements of their physico-chemical properties, collectively contains valuable chemical information on the atomic bonding and structure-property relations of these nanomaterials, which could be used for successful structural predictions of yet unknown nanoparticles. Here, we devise and demonstrate a general method for predicting metal-ligand interface structures of an unknown ligand-protected metal nanocluster. Our method is based on a local search algorithm that uses information about the known local atomic environments at the metal-ligand interface of reference nanostructures in the same class of hybrid nanoparticles. The specific example systems discussed in this work comprise gold (Au) and silver (Ag) nanoclusters protected by thiols (SR), phosphines (PR_3) and diphosphines (DPPY), and we demonstrate how experimentally verified Au/Ag-thiolate and Ag-phosphine interface structures can be successfully built when the positions of all Au or Ag atoms in the cluster are first defined. However, the method itself is general and can be used for any type of nanoparticle or nanostructure if enough reference structural information is available in the same class of systems. The set of reference structures can be considered as a training set and the whole procedure to refine the candidates for the metal-ligand interfacial structures may be considered as an analogue to applying machine learning methodology to the structure prediction problem.[12]

Results

Structure prediction algorithm. Our procedure to build candidates for the atomic structure of gold-sulfur interfaces is summarized in Algorithm 1 (in Methods) and Figure 1. The main algorithm is divided into steps 0-4 as follows (the steps are also numbered the same way in Figure 1).

1. First, a group of known reference structures (training set) is defined. The training set may include experimental crystal structures, computational model structures, partial structures, or hand-made intuitive structural guesses.

2. The coordinates for the metal atoms (here Au or Ag) are set. This information may come, *e.g.,* from experimental electron microscopy data.

3. A list of possible positions for interface atoms (here S or P) around the metal core is built. The local chemical bonding determines the acceptance of a point of a dense grid (Supplementary Fig. 1) as a possible interface atom position, based on comparison to bond lengths and angles found in the training set (Supplementary Note 4 and Supplementary Fig. 2). In addition, a spatial fitting of the molecule (ligand) attached to the interface is required for acceptance. Here, fitting of the organic part of thiolates and phosphines is tested with a specific sized rigid sphere in the most prominent bonding direction with respect to the nearest neighbour Au-S, Ag-S or Ag-P bonds as visualized in Figure 2. Finally, the list of all possible interface atom positions is saved and used as a basis for the random multi-start selection process in step 3.

4. N complete interface structures are created from the possible interface atom positions by a restricted random multi-start selection process as described in Algorithms 2-4 (see Methods). The restrictions are based on simple rules of chemistry related to coordination, atomic distances and local conformations (see Methods, Supplementary Note 2, and Figure 2). The process starts by adding randomly picked interface atoms, from the list generated in step 2, first into specified local conformations such as linear SR-Au/Ag-SR arrangements resembling a part of protecting SR-(Au/Ag-SR)$_n$ (n=1,2) units (Figure 2). The protecting units are the main components forming the gold-thiolate interface structure in many known thiolate-protected gold clusters. For protected Ag-clusters, more than one local structural arrangement is possible with respect to

SR-Ag-SR angles because of the more flexible Ag-S coordination compared to gold (see Figure 2 and Supplementary Fig. 3). In the case diphosphines, the specified local conformation is a pair of phosphorus atoms, for which the P-P distance is restricted based on the connecting organic group between the phosphine ends of the molecule. Next, single thiolates or single phosphines will be used to fill the remaining free metal surface if necessary. The selection process ends when there are no valid points left in the list of possible interface atom positions. All selected interface atom coordinates form one potential model structure. The total number of generated model structures should be set large enough to overcome the challenges of a non-guided stochastic process to represent all relevant overall interface conformations.

5. The final step of the algorithm ranks the generated model structures. For the ranking we introduce a numerical criterion, a so-called Combined Structural Error (CSE) (see the full description in Supplementary Note 1), which is constructed as an average from the errors related to the nearest neighbor bonds and angles, to the number of predicted interface atoms in specified local conformations, and to the total number of interface atoms. Experimental evidence indicates that the most stable ligand protected gold and silver clusters also have the most complete steric protection of the metal core by the ligand layers. After ranking, the best model structures can be completed by adding the organic part of the ligand layer and optimizing the atomic structure of the ligand layer by molecular mechanics or molecular dynamics. One possible approach is demonstrated in our previous work.[13]

A working strategy to avoid stochastic challenges (non-effective random search of possible ligand atom positions for larger clusters) is discussed in Supplementary Note 2. Criteria for selecting the geometric parameters for step 2 above are discussed in Supplementary Note 3.

Reference structures and validation of the algorithm. For Au-S interface prediction, the set of reference structures included 24 known protected gold nanoclusters $Au_x(SR)_y$ between the sizes $(18,14) \leq (x,y) \leq (279,84)$ as well as the short RS-Au-SR and longer RS-Au-SR-Au-SR unit conformations

(Supplementary Figure 3). For Ag-S and Ag-P interfaces, 17 known thiolate and/or phosphine protected silver nanoclusters were included in the set of reference structures. The reference silver nanoclusters have 14 – 374 Ag-atoms and 20 – 117 ligands including thiolates, phosphines, diphosphines and halides. A complete list of the reference structures is given in Supplementary Note 4. Based on the reference information, the algorithm was validated for protected Au-S interfaces by examining 10 $Au_x(SR)_y$ clusters in the range $(34,22) \leq (x,y) \leq (279,84)$ where the structure is known experimentally,[14-23] removing the ligand layer including sulfurs, by building a large number of potential structures of the ligand layer around the fixed gold core, ranking the structures, and comparing these Au-S interface structures with the experimental crystal structure. Validation in the case of Ag-S interfaces was done with four protected Ag-clusters in the size range of 23-211 Ag-atoms and 26-78 ligands.[24-27] Two of these clusters had ligand layers consisting of both thiolates and phosphines, and one consisting of thiolates and diphosphines. Combined, the selected Au- and Ag-clusters include various different symmetries, cluster sizes, surface curvatures, surface morphologies, and protecting ligand motifs. Table 1 and Supplementary Tables S1-S6 give the full structural details and parameters related to the prediction and validation. The cluster that was predicted was excluded from the reference structures in each example.

Prediction of Au-S interface structure for ligand protected gold clusters. To test and validate our algorithm for Au-S interfaces, we selected 9 known clusters: $Au_{34}(SR)_{22}$ (ref. 14), $Au_{36}(SR)_{24}$ (ref. 15), $Au_{38}(SR)_{24}$ (ref. 16), $Au_{44}(SR)_{26}$ (ref. 17), $Au_{52}(SR)_{32}$ (ref. 18), $Au_{92}(SR)_{44}$ (ref. 19), $Au_{102}(SR)_{44}$ (ref. 20), $Au_{146}(SR)_{57}$ (ref. 21), and $Au_{279}(SR)_{84}$ (ref. 22). In addition, $Au_{44}(SR)_{28}$ cluster[23] was also used for analyzing the ligand size effects at the interface as discussed later. The summary of the parameters used in prediction are given in Supplementary Table 1. The test systems include various different ligand layer conformations consisting of different length of $SR-(Au-SR)_n$ protecting units and single bridged thiolates. For all clusters, 9216 model structures were generated in a single run, and for the two largest clusters $Au_{146}(SR)_{57}$ and $Au_{279}(SR)_{84}$ the prediction was done twice by combining the sulfur atom positions of 20 best model structures of the first round into a new set of possible S-atom positions for the second round. 20 best model structures were taken from those that had the largest number of ligands in units and in total in the first round. Furthermore, correct structures were determined by comparing the atomic indices of the two nearest neighbor Au-atoms of each sulfur of the model structure with respect to the nearest sulfur atom of the true known structure.

Table 1 shows the results. The success of prediction was determined as a ratio of the correct structures to all generated model structures, varying notably much, from 0.67% to 94.0%. The maximum number of S-atoms found in the protecting units and in total are in a very good agreement with the compositions of the true structures. This indicates that the true stable structures maximize the number of ligands on the surface to best protect the metal core from the degradation. The lowest RMSD (root mean square deviation) values of the correct model structures range from 0.261 Å to 0.545 Å, and the corresponding structures are shown in Figure 3. The algorithm is flexible to be used with different kind of sets of reference structures, as indicated for $Au_{102}(SR)_{44}$, where only conformations of one short SR-Au-SR unit and one long unit SR-Au-SR-Au-SR unit (Supplementary Figure 3) were used successfully for the prediction. For all other systems the complete set of reference structures were used omitting always the cluster in question as listed in Supplementary Note 4.

The ratio of correct S-atom positions as a function of CSE is shown for all of the examined protected Au-clusters in Figure 4. The correctly positioned atoms were determined similarly as in Table 1. For all systems in panels a-i of the Figure 4 the ratio of correct atoms approaches 1.0 when CSE gets smaller. For most of the investigated systems, the model structure with a minimum CSE value matches with the true structure by nearest neighbor bonding, except in the most challenging case of $Au_{279}(SR)_{84}$, where the true structure is found among 5-10 best model structures. For the CSE, 5 nearest neighbors were used for describing the local environment of atoms and for all systems the corresponding error was calculated with respect to the same set of reference structures that was used in the model structure generation. Noteworthy is that the CSE separates the correct structure of $Au_{102}(SR)_{44}$ regardless of the fact that the set of reference structures is considerably smaller, although the observed range of the CSE, 0.26-0.46, reflects the incompleteness of the set of reference structures used in the prediction. For the clusters which have comparable decent set of reference structures, the minimum CSE values are found consistently between 0.04-0.06 regardless of the size of the system. The ratio of correct atoms on the surface depends on the other hand on the complexity of the investigated system. For the simplest systems such as $Au_{38}(SR)_{24}$, all the generated model structures have >85% of the added S-atoms correct but for example for the similar sized cluster $Au_{36}(SR)_{24}$ the range is 30% - 100%.

The structures of $Au_{44}(SR)_{26}$, $Au_{92}(SR)_{44}$, $Au_{146}(SR)_{57}$ and $Au_{279}(SR)_{84}$ have single bridged ligands that do not resemble the arrangement of protecting units. The number of bridged ligands added on the

surface of each of these clusters is in the range of 2-18 and can be seen from the difference of the number of ligands in total and in the units shown in Table 1. For some of the systems the total number of the interface atoms added on the surface exceeds the true number of ligands, but regardless of that the algorithm is accurate enough for predicting both the number and the positions of the bridge ligands by the ranking criteria. These results confirm that in the true structures the number of interface atoms in linear SR-Au-SR conformations is often maximized. This is automatically taken into account in the design of the Algorithm and is also build into the CSE measuring the goodness of the model structures.

Prediction of Ag-S interface structure for ligand protected silver clusters. The main difference when predicting Ag-S interface as compared to predicting Au-S interface is to allow more flexible coordination of the metal atoms to thiolates. The selected parameters for protected Ag-clusters can be seen in Supplementary Table 2. For validating the prediction of Ag-S interface structures we selected four known protected Ag-clusters: $Ag_{23}(SR)_{18}(PPh_3)_8$ (ref. 24), $Ag_{44}(SR)_{30}$ (ref. 25), $Ag_{78}(SR)_{42}(DPPP)_6$ (ref. 26), and $Ag_{211}Cl(SR)_{71}(PPh_3)_6$ (ref. 27). For these clusters most of the ligands on the surface are thiolates, but also phosphines, diphosphines and one halide are included. The single halide is omitted in the prediction. Our approach to predict the interfaces with mixed ligands is to predict first the positions of the ligands that are in majority and then to continue by predicting the other ligands, in this case phosphines and diphosphines. For all test systems, 9216 model clusters were generated during a single run. The prediction was done twice for the largest $Ag_{211}Cl(SR)_{71}(PPh3)_6$ cluster by combining the S-atom positions of 20 best structures of the first run to the set of possible S-atom positions for the second run, similarly to the two largest Au-clusters discussed above. The correctly positioned atoms were determined by requiring that 4 out of 5 nearest neighbors metal atom indices must be correct for all interface atoms as compared to the true structure. This criterion is different than in Au-S interfaces due to the enriched bonding configurations on Ag-S interface, for which taking into account only 2 nearest neighbors would not be enough.

Table 1 shows the results from prediction for all four systems. The success of the prediction varies from 0.022 % to 42.9 %. To remark, the success ratio increased from 0% to 0.85% for the largest cluster Ag_{211} from the first to the second prediction run. The maximum number of ligands found in protecting units and in total are in a very good agreement with the molecular compositions of the true structures for all systems. The minimum RMSD values of the correct structures are in range 0.225 Å –

0.744 Å and the corresponding structures are shown in Figure 5. The Ag-S interfaces are more complex than Au-S interfaces especially in larger clusters which can be seen as a more significant variations in the positions of the sulfur atoms compared to the true structure and also in the success rates and the RMSD values.

CSE is efficient also for predicting the true structures for protected Ag-clusters as can be seen from Figure 6 for the four studied cases. Similarly to Au-clusters, the model structures that have the smallest CSE values include most probably the true structure. It is interesting to note that even for the clusters with mixed ligand layers of thiolates and phosphines the true Ag-S part of the overall interface conformation can be predicted before addition of the phosphines or diphosphines. This enables prediction of the overall conformations of the metal-ligand interfaces in steps, first for the ligands that are in majority and then continuing the process with the ligands in minority for the best structures. Completing the prediction with phosphines and diphosphines is described next.

Predicting phosphine positions for the mixed ligand silver clusters. Predicting Ag-P interface for the clusters with mixed ligand layers of thiolates and phospines or thiolates and diphosphines was done by starting from one of the correctly predicted partial structures based on the Ag-S interface predictions. Both Ag-atom and S-atom positions are included when describing the local environments for the phosphorus atoms. To accomplish this, atom types were also included the nearest neighbor description when searching the possible interface atom positions. The parameters used in prediction of Ag-P interface are given in Supplementary Table 3. For all clusters we used systematically 4 nearest neighbors with 0.1-0.2 Å error limits for the distances and 10 degrees limit for the angles. One of the clusters have diphosphines instead of phosphines for which the single P atoms are added in pairs by restricting the distance to a range 5.0 – 5.5 Å based on the length of the carbon chain between the phosphine ends in the molecule (see Figure 2). The spatial fitting of the organic groups (e.g. triphenyl) were done by one large spherical probe in parallel direction to the nearest neighbor Ag-P bond.

The results for the Au-P interface are shown in the Supplementary Table 4 and the P-atom positions in the best structures in Figure 5. For all the clusters the success of prediction is perfect: 100% out of all 3072 model structures were correctly built. The prediction of phosphines is easier compared to thiolates due to the diminished number of possible local conformations. In general, phosphines tend to bind into

a tetrahedral arrangement with respect to the nearest neighbor Ag-atom and the three nearest S-atoms as shown in Figure 2. To describe this kind tetrahedral arrangement, at least 4 nearest neighbors were needed for the local environment description.

Correlation of the combined structural error to DFT total energy. It is interesting to correlate the CSE values to the DFT total energies for a group of generated model structures. We investigated this in the case of those $Au_{36}(SR)_{24}$ model structures that have the molecular composition of the true cluster but not necessarily the true structure. DFT total energies of 700 model structures were calculated by describing the thiolates by simplified SH-groups added in the perpendicular direction to the nearest neighbor Au-S bonds of each predicted S-atom with a bond distance of 1.368 Å. For the analysis, we averaged the CSE of the individual model clusters within increments of 0.4 eV with respect to the total energies. The correlation of the averaged CSE to the total energy is shown in Figure 7. The result shows a clear trend: the total energy decreases when the CSE decreases. This confirms that the minimum energy structures can be found most probably among the model structures that have low CSE values. The larger fluctuations at low and high energies seen in Figure 7 are related to the decreased number of model clusters in sampling on both extremes. This comparison confirms the validity of CSE in predicting the true structure.

Explaining the size effects of the ligands in thiolate protected Au_{44} clusters. The ligand size (steric volume) is one of the properties affecting the possible S- or P-atom positions on the metal surface. There are several examples of protected Au-clusters for which isomeric structures with different geometries are found with ligands of different bulkyness. Even cluster transformations driven by a ligand exchange from non-bulky to bulky ligand have been reported. Our algorithm provides a possibility to qualitatively study and understand the triggering conditions for these experimental findings. As an example, two different experimentally known thiolate protected Au_{44} clusters have been reported: one with 26 and the other with 28 thiolates from which the first is made with tertbutylbenzenethiol (TBBT) and the second with dimethylbenzenethiol (DMBT).[17,23] These two clusters are completely different by the metal core symmetry and metal-ligand interface structures. Here we tested our algorithm whether it can predict that the true structure and composition of the $Au_{44}(SR)_{28}$ is achieved only for TBBT ligand and not for the larger DMBT. The parameters used in the prediction and the results are summarized in Supplementary Tables 5 and 6. By varying the radius of

the spherical probe from 2.5 Å (for modeling TBBT) to 3.0 Å (DMBT), the maximum number of thiolates at the interface drops from 28 to 26 (Figure 8). The largest ligand that may occupy full 28 ligand sites on the surface corresponds to a 2.8 Å sized spherical probe. Remarkably, this in a perfect match with the true experimentally observed composition of DMBT protected Au-cluster. This can be understood by a competing effects from the interactions of the metal core and the metal-ligand interface and the spatial fitting of organic ligands, both affecting the overall structure. Since the metal core size is almost the same for both clusters and the metal atoms tend to maximize the packing of the core, there is roughly the same amount of free space for the ligands on the surface. This free space gets filled with 26 DMBT ligands if proper parameters for its steric volume are used.

Discussion

In this work, we have introduced a general method that can be used to predict metal-ligand interface structures of ligand protected metal nanoparticles. The method uses the information from the local bonding environments of known reference structures (in our case the reference structures comprise reported crystal structures of similar thiolate- and phosphine-protected gold and silver nanoclusters) and can be easily generalized for the structural prediction of any nanostructure, in case enough reference information is available. The main variables, nearest neighbour bonds and bond angles between the interface atoms, are generally valid to be used for any atom type in any nanostructure. The steric parameters used in this paper can easily be generated to any atom types and molecular groups at the metal-ligand interface. Our algorithm is written in a modular way in order to maximize the flexibility and transferability to other metal-ligand systems, such as gold-alkynyls etc. An interesting test case would be provided by predictions of gold-thiolate interfacial structures in planar, self-assembling thiol monolayers on Au(111), which has been under intense investigations since 1980's.[28,29]

We validated the method by predicting the Au-S interface structures of 10 known thiolate-protected gold nanoclusters and the Ag-S and Ag-P interface structures of 4 known ligand protected silver clusters. Furthermore, we introduced a CSE parameter to measure the goodness of generated model clusters showing a clear correlation of low CSE value to low DFT total energy. The definition of CSE enables additional terms or "fitness functions" including both local and global descriptors, which could relate to structure-dependent properties such as X-Ray powder diffraction patterns.

In all studied cases, the best-ranked structures essentially reproduced the bonding configuration of metal-ligand interfaces found in the crystal structure, with minor RMSD values in the predicted interface atom positions with respect to the crystal structure. We successfully predicted also the metal-ligand interfaces consisting of different kind of ligands (thiolates and phosphines), for which the prediction was made in steps by first predicting the most stable configurations of thiolates that are in majority and then predicting the positions of the phosphines that were in minority. In general, we expect that by applying structure optimization methods, a majority of the best model structures would relax to the known experimental structure. For the largest clusters studied in this work we also expect that a number of predicted best-ranked interface structures would lead to locally stable low-energy isomers lying energetically close to the known crystal structure. In this sense, our method should be useful in producing a number of potential structural isomers in a systematic and computationally effective way. These isomeric structures can then be examined with more robust energy-optimization methods such as DFT or DFT-based tight-binding methods. Since the spatial constraints from the ligand layer (*i.e.,* the steric volume of the ligand molecule) are also parametrically included in the algorithm, we showed that our method can provide qualitative understanding on how the bulkiness of the ligand affects structures, interface conformations and compositions of the protected clusters.

Our experience on this method implies three critical points of concern to be adjusted to the system under investigation, to guarantee the success of the structure-prediction algorithm. First, a large enough sampling of the plausible local structures is needed in the set of reference structures. Second, the interval between grid points (Supplementary Fig. 1) has to be chosen fine enough. In this work, we used a value of 0.2 Å. Third, too loose criteria for describing the local environments of atoms may lead to improper bonding configurations that deviate from the true metal-ligand chemistry. We found reasonable to allow up to about 10% error in S-Au bond length and in RS-Au-SR angles depending on the number of nearest neighbors considered in the description. All the parameters we used were based on statistical analysis of experimental structural data of a similar class of clusters in question.

Unguided stochastic process starts to dictate the generation of the model structures for larger systems so that ever larger number of model structures have to be generated in order to have a complete representation of all relevant overall conformations. A further advantage of our method is that the process can be made guided by weighting the good choices made in model structure generation. In this study we introduced one possible approach for optimizing the global structural search. The main idea is

to repeat the predictions by taking for the next run the possible interface atom positions from the set of best model structures of the previous run. Other possibilities would be to weight the interface atom positions on-the-fly based on the success of the model structure generation.

Our future work will be directed to developing more numerically effective methods for evaluating the candidate structures, which eventually could reduce the need to use a large number of heavy total energy evaluations at the DFT level. Our goal is also to extend the structural prediction of metal-ligand interfaces into the metal atoms and complete cluster structures. We hope that the method described in this work can open new avenues for effective structural predictions of nanoparticles and more generally nanomaterials where the atomic-scale information of the metal-ligand interface is crucial to understand growth mechanisms, stability, dynamics and ensuing physico-chemical properties. As such, our work is complementary to recent efforts to develop understanding of gold nanoparticle synthesis via deep learning.[30]

Methods

The main features of our method are described in the main text and the corresponding algorithms are given here. The main Algorithm 1 depends on Algorithms 2-4 described. The physico-chemical reasons for the selected parameters used in the prediction algorithm are discussed in the main text.

The approach to use a greedy enlargement during the search resembles the classical graph traversal algorithms.[31] Such approaches form part of the search-based artificial intelligence as suggested by Nielsen.[32]

DFT method. The density functional theory (DFT) calculations were run using the GPAW code-package[33] with the grid spacing of 0.2 Å and Perdew-Burke-Ernzerhof (PBE) xc-functional.[34] DFT total energies were calculated without structure relaxation from a set of 700 generated model structures of $Au_{36}(SR)_{24}$ cluster by adding the ligands as simplified SH-groups in the most natural bonding direction using the optimal bond distance. In practice, it means adding H-atoms perpendicular to the nearest neighbor Au-S bonds with the S-H bond distance of 1.368 Å. Total energies were used for studying the correlation to the combined structural error (CSE), which was averaged in increments of 0.4 eV of total energy.

Algorithm 1 Create a model structure

Require: Database of reference structures (training set)
Ensure: Set of model structures for the metal-ligand interface

1: Define coordinates of metal atoms
2: Find possible interface atom positions around the metal atoms, using information about the local chemical environments in the training set
3: **for** N times **do**
   Generate a random, plausible model structure
4: Rank each model structure based on selected criteria, and select the best one(s)

Algorithm 2 Generate a random, plausible model structure

Require: Coordinates of metal atoms G_{M0}, initial plausible interface atom positions G_{S0}, minimum distance of isolated interface atoms $d_{LL,2}$
Ensure: a random plausible model structure, final coordinates of interface atoms G_{Sf}

1: $G_{Si} \leftarrow G_{S0}$
2: $G_{Sf} \leftarrow \emptyset$
3: **while** $G_{Si} \neq \emptyset$ **do**
4: $\quad p_{i1} \leftarrow random(G_{Si})$
5: $\quad (G_{Si}, G_{Sf}) \leftarrow TryLocalStruct(p_{i1}, G_{Si}, G_{Sf}, G_{M0})$
6: $\quad G_{Si} \leftarrow RemoveImpossible(G_{Si}, G_{Sf}, G_{M0})$
7: $\quad G_{Si} \leftarrow \{p_j : p_j \in G_{si}; p_j \neq p_{i1}\}$
8: $G_{Si} \leftarrow G_{S0}$
9: **for** $p_f \in G_{Sf}$ **do**
10: $\quad G_{Si} \leftarrow G_{Si} \setminus \{p_j : p_j \in G_{Si}; d(p_j, p_f) < d_{LL,2}\}$
11: $G_{Si} \leftarrow RemoveImpossible(G_{Si}, G_{Sf}, G_{M0})$
12: **while** $G_{Si} \neq \emptyset$ **do**
13: $\quad p_i \leftarrow random(G_{Si})$
14: $\quad G_{Sf} \leftarrow G_{Sf} \cup \{p_i\}$
15: $\quad G_{Si} \leftarrow G_{Si} \setminus (\{p_i\} \cup \{p_j : p_j \in G_{Si}; d(p_j, p_i) < d_{LL,2}\})$
16: $\quad G_{Si} \leftarrow RemoveImpossible(G_{Si}, G_{Sf}, G_{M0})$

Algorithm 3 $TryLocalStruct(p_{i1}, G_{Si}, G_{Sf}, G_{M0})$ //
Add specified local structure if possible and remove positions based on distances

Require: Trial interface atom coordinate $p_{i1} \in G_{Si}$, initial plausible interface atom positions G_{Si}, final selected interface atom positions G_{Sf}, coordinates of metal atoms G_{M0}, minimum distance of interface atoms of specified local structure $d_{LL,1}$, possible bond angles α_i and error $\Delta\alpha_i$ between two interface atoms and the nearest metal atom in the local structure.

Ensure: Updated initial plausible interface atom positions G_{Si}, updated final coordinates of interface atoms G_{Sf}

for $p_M \in \{p_{Mj} : p_{Mj} \in G_{M0}; d(p_{Mj}, p_{i1}) \in [1.95\text{Å}, 2.75\text{Å}]\}$ **do**
  $G_1 \leftarrow \{p_j : p_j \in G_{Sf}; d(p_j, p_M) \in [1.95\text{Å}, 2.75\text{Å}] \bigwedge \theta(p_{i1}, p_M, p_j) \in [\alpha_i - \Delta\alpha_i, \alpha_i + \Delta\alpha_i]\}$
  if $G_1 \neq \emptyset$ **then**
    $G_{Sf} \leftarrow G_{Sf} \cup \{p_{i1}\}$
    $G_{Si} \leftarrow G_{Si} \setminus (\{p_{i1}\} \cup \{p_j : p_j \in G_{Si}; d(p_j, p_{i1}) < d_{LL,1}\})$
    break
  else
    $G_2 \leftarrow \{p_j : p_j \in G_{Si}; d(p_j, p_M) \in [1.95, 2.75] \bigwedge \theta(p_{i1}, p_M, p_j) \in [\alpha_i - \Delta\alpha_i, \alpha_i + \Delta\alpha_i]\}$
    if $G_2 \neq \emptyset$ **then**
      $p_{i2} \leftarrow SelectFirst(G_2)$ // (first member of the set)
      $G_{Sf} \leftarrow G_{Sf} \cup \{p_{i1}, p_{i2}\}$
      $G_{Si} \leftarrow G_{Si} \setminus (\{p_{i1}, p_{i2}\} \cup \{p_j : p_j \in G_{Si}; d(p_j, p_{i1}) < d_{LL,1} \bigvee d(p_j, p_{i2}) < d_{LL,1}\})$
      break

Algorithm 4 $RemoveImpossible(G_{Si}, G_{Sf}, G_{M0})$ //
Remove initial positions based on metal atom coordination

Require: Initial plausible interface atom positions G_{Si}, final selected interface atom positions G_{Sf}, coordinates of metal atoms G_{M0}, maximum coordination of metal atoms $cnumb_{max}$

Ensure: Updated initial plausible S-atom positions G_{Si}

for $p_M \in G_{M0}$ **do**
  $cnumb \leftarrow size(\{p_f : p_f \in G_{Sf}; d(p_f, p_M) < 2.75\text{Å}\})$
  if $cnumb \geq cnumb_{max}$ **then**
    $G_{Si} \leftarrow G_{Si} \setminus \{p_j : p_j \in G_{Si}; d(p_j, p_M) < 2.75\text{Å}\}$

Data and code availability. The algorithm published in this work is fully documented in the main text and in the Supplementary Information. All the reference structural data was taken from previously published work and referenced accordingly. The software and examples of full datasets/runs for the examined cases that validated our method are available by request to H.H.

References

1. Daniel, M.-C. & Astruc, D. Gold nanoparticles: Assembly, supramolecular chemistry, quantum-size-related properties, and applications toward biology, catalysis, and nanotechnology. *Chem. Rev*. **104**, 293–346 (2004).
2. Boisselier, E. & Astruc, D. Gold nanoparticles in nanomedicine: preparations, imaging, diagnostics, therapies and toxicity. *Chem. Soc. Rev*. **38**, 1759-1782 (2009).
3. Tsukuda, T. & Häkkinen, H. Protected metal clusters: From fundamentals to applications. Elsevier, Amsterdam 2015.
4. Zhang, Y.W., Song, P., Chen, T., Liu, X., Wu, Z., Wang, Y., Xie, J. & Xu, W. Unique size-dependent nanocatalysis revealed at the single atomically precise gold cluster level. *Proc. Natl. Acad. Sci (USA)* **115**, 10588-10593 (2018).
5. Weerawardene, K.L., Dimuthu, M., Häkkinen, H. & Aikens, C.M. Connections between theory and experiment for gold and silver nanoclusters. *Annu. Rev. Phys. Chem*. **69**, 205-229 (2018).
6. Chakraborty, I & Pradeep, T. Atomically precise noble metals: Emerging link between atoms and nanoparticles. *Chem. Rev*. **117**, 8208-8271 (2017).
7. Marjomäki, V., Lahtinen, T., Martikainen, M., Koivisto, J., Malola, S., Salorinne, K., Pettersson, M. & Häkkinen, H. Functionalized gold clusters as site-specific labels for imaging of enteroviruses. *Proc. Natl. Acad. Sci (USA)* **111**, 1277-1281 (2014).
8. Azubel, M., Carter, S.D., Weiszmann, J., Zhang, J., Jensen, G.J., Li, Y. & Kornberg, R.D. FGF21 trafficking in intact human cells revealed by cryo-electron tomography with gold nanoparticles. *ELIFE* **8**, e43146 (2019).
9. Azubel, M., Koivisto, J., Malola, S., Bushnell, D., Hura, G.L., Koh, A.L., Tsunoyama, H., Tsukuda, T., Pettersson, M., Häkkinen, H. & Kornberg, R.D. Electron microscopy of gold nanoparticles at atomic resolution. *Science* **345**, 909-912 (2014).
10. Azubel, M., Koh, A.L., Koyasu, K., Tsukuda, T. & Kornberg, R.D. Structure determination of a water-soluble 144-gold atom particle at atomic resolution by aberration-corrected electron microscopy. *ACS Nano* **11**, 11866-11871 (2017).
11. Billinge, S. & Levin, I. The problem with determining atomic structure at the nanoscale. *Science* **316**, 561–565 (2007).
12. Schneider, W. F. & Guo, H. Machine learning. *J. Phys. Chem. A* **122**, 879–879 (2018).
13. Tero, T.-R., Malola, S., Koncz, B., Pohjolainen, E., Lautala, S., Mustalahti, S., Permi, P., Groenhof, G., Pettersson, M. & Häkkinen, H. Dynamic stabilization of the ligand-metal interface in atomically precise gold nanoclusters Au68 and Au144 protected by meta-mercaptobenzoic acid. *ACS Nano* **11**, 11872– 11879 (2017).
14. Dong, H., Liao, L., Zhuang, S., Yao, C., Chen, J., Tian, S., Zhu, M., Liu, X., Li, L. & Wu. Z. A novel double-helical-kernel evolution pattern of gold nanoclusters: alternate single-stranded growth at both ends, *Nanoscale* **9**, 3742-3746 (2017).
15. Zeng, C., Qian, H., Li, T., Li, G., Rosi, N. L., Yoon, B., Barnett, R. N., Whetten, R. L., Landman, U. & Jin, R. Total Structure and Electronic Properties of the Gold Nanocrystal Au36(SR)24. *Angew. Chemie Int. Ed.* **51**, 13114–13118 (2012).
16. Qian, H., Eckenhoff, W.T., Zhu, Y., Pintauer, T. & Jin, R. Total Structure Determination of Thiolate-Protected Au38 Nanoparticles. *J. Am. Chem. Soc*. **132**, 8280–8281 (2010).

17. Liao, L., Zhuang, S., Yao, C., Yan, N., Chen, J., Wang, C., Xia, N., Liu, X., Li, M-B., Li, L., Bao, X. & WuZ. Structure of chiral Au44(2,4-DMBT)26 nanocluster with an 18-electron shell closure. *J. Am. Chem. Soc*. **138**, 10425-10428 (2016).
18. Zhuang, S., Liao, L., Li, M.-B., Yao, C., Zhao, Y., Dong, H., Li, J., Deng, H., Li, L. & Wu. Z. The fcc structure isomerization in gold nanoclusters. *Nanoscale* **9**, 14809-14813 (2017).
19. Zeng, C., Liu, C., Chen, Y., Rosi, N.L. & Jin, R. Atomic structure of self-sssembled monolayer of thiolates on a tetragonal Au92 nanocrystal. *J. Am. Chem. Soc.* **138**, 8710–8713 (2016).
20. Jadzinsky, P.D., Calero, G., Ackerson, C.J., Bushnell, D.A. & Kornberg, R.D. Structure of a thiol monolayer-protected gold nanoparticle at 1.1 Ångstrom resolution. *Science* **318**, 430-433 (2007).
21. Vergara, S., Lukes, D.A., Martynowycz, M.W., Santiago, U., Plascencia-Villa, G., Weiss, S.C., de la Cruz, M.J., Black, D.M., Alvarez, M.M., Lopez-Lozano, X., Barnes, C.O., Lin, G.W, Weissker, H.C., Whetten, R.L., Gonen, T., Yacaman, M.J. & Calero, G. MicroED structure of Au_{146}(p-MBA)$_{57}$ at subatomic resolution reveals a twinned FCC cluster. *J. Phys. Chem. Lett*. **8**, 5523–5530 (2017).
22. Sakthivel, N. A., Theivendran, S., Ganeshraj, V., Oliver, A. G. & Dass, A. Crystal structure of faradaurate-279: Au279 plasmonic nanocrystal molecules. *J. Am. Chem. Soc*. **139**, 15450–15459 (2017).
23. Zeng, C., Chen, Y., Iida, K., Nobusada, K., Kirschbaum, K., Lambright, K.J. & Jin. R. Gold quantum boxes: On the periodicities and the quantum confinement in the Au28, Au36, Au44, and Au52 magic series. J. *Am. Chem. Soc.* **138,** 3950–3953 (2016).
24. Liu, C., Li, T., Abroshan, H., Li, Z., Zhang, C., Kim, H.J., Li, G. & Jin, R. Chiral Ag23 nanocluster with open shell electronic structure and helical face-centered cubic framework, *Nature Comm.* **9**, 744 (2018).
25. Yang, H., Wang, Y., Huang, H., Gell, L., Lehtovaara, L., Malola, S., Häkkinen, H. & Zheng, N. All-thiol-stabilized Ag44 and Au12Ag32 nanoparticles with single-crystal structures. *Nature Comm.* **4**, 2422 (2013).
26. Yang, H., Yan, J., Wang, Y., Deng, G., Su, H., Zhao, X., Xu, C., Teo, B.K. & Zheng, N. From racemic metal nanoparticles to optically pure enantiomers in one pot. *J. Am. Chem. Soc.* **139**, 16113-16116 (2017).
27. Liu, J.Y., Alkan, F., Wang, Z., Zhang, Z.-Y., Kurmoo, M., Yan, Z., Zhao, Q.-Q., Aikens, C.M., Tung, C.-H., Sun, D. Different silver nanoparticles in one crystal: Ag210(iPrPhS)71(Ph3P)5Cl and Ag211(iPrPhS)71(Ph3P)6Cl. *Angew. Chemie* **58**, 195-199 (2019).
28. Love, J., Estroff, L.A., Kriebel, J.K., Nuzzo, R.G. & Whitesides, G.M. Self-assembled monolayers of thiolates on metals as a form of nanotechnology. *Chem. Rev*. **105**, 1103-1169 (2005).
29. Häkkinen, H. The gold-sulfur interface at the nanoscale. *Nature Chem*. **4**, 443-455 (2012).
30. Li, J., Chen, T., Lim, K., Chen, L., Khan, S.A., Xie, J. & Wang, X. Deep learning accelerated gold nanocluster synthesis. Preprint at: https://arxiv.org/abs/1811.02771
31. Dijkstra, E.W. A note on two problems in connection with graphs. *Num. Math.* **1**, 269-271 (1959).

32. Nilsson, N.J. Principles of Artificial Intelligence. Springer, Berlin 2014.
33. Enkovaara, J. et al., Electronic Structure Calculations with GPAW: A Real-Space Implementation of the Projector Augmented-Wave Method, *J. Phys. Condens. Matt*. **22**, 253202 (2010).
34. Perdew, J.P., Burke, K & Ernzerhof, M. Generalized Gradient Approximation Made Simple, *Phys. Rev. Lett.* **77**, 3865-3868 (1996).

Acknowledgements

This work was supported by Academy of Finland through the AIPSE research program, grants 315549 (H.H.), 315550 (T.K.) and 311877 (T.K.), and through H.H.'s Academy Professorship. The computations were made using resources at the Nanoscience Center (NSC) of University of Jyväskylä and at the CSC supercomputing center in Finland.

Author contributions

S.M. and H.H. conceived the concept, S.M. built the structure prediction algorithm, validated the results and wrote the first draft of the manuscript. A.P., P.N., J.H. and T.K. contributed in the development of the algorithm. H.H. supervised the work. All authors commented on the manuscript draft that was finalized by H.H.

Additional information

Supplementary Information accompanies this paper at http://www.nature.com/naturecommunications

Competing interests: The authors declare no competing interests.

Reprints and permission information is available online at http://npg.nature.com/reprintsandpermissions/

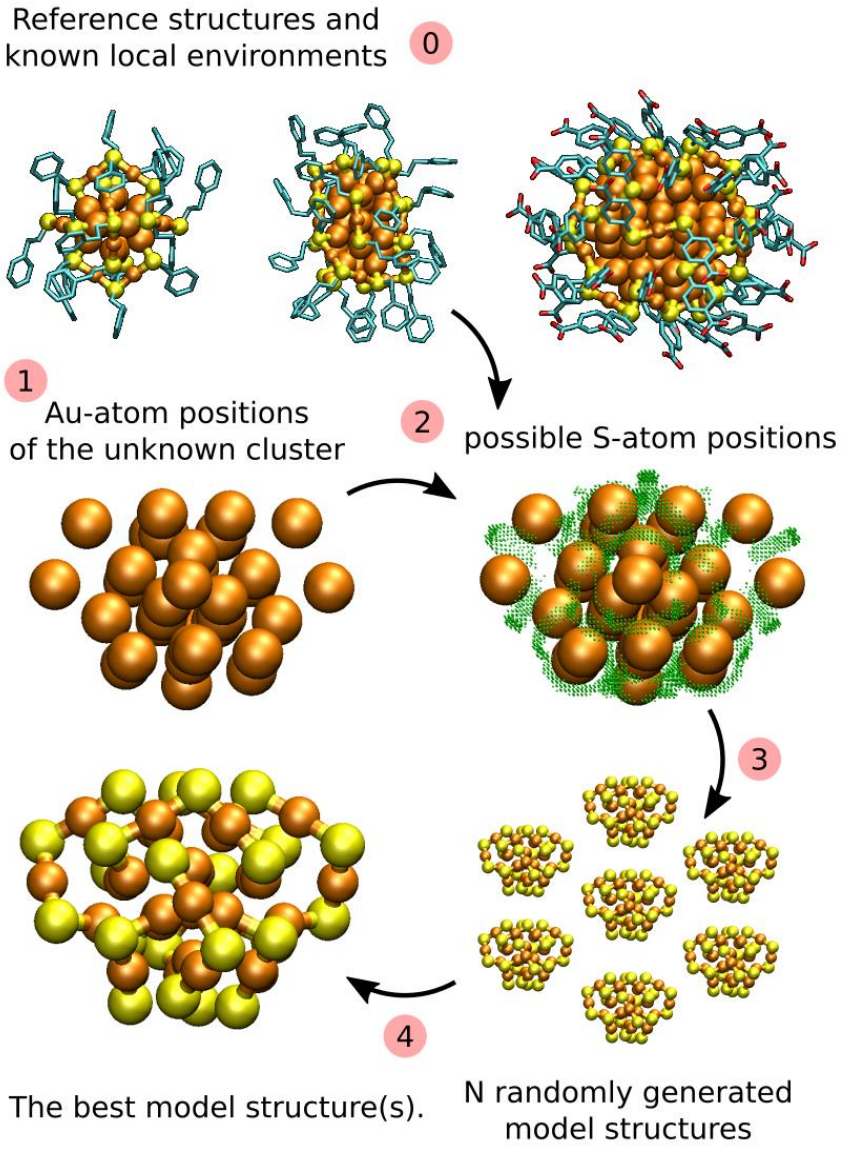

Figure 1 | A schematic visualization of the algorithm. Using a set of reference structures of known $Au_x(SR)_y$ nanoclusters, several candidates for the structure of the layer of sulfur atoms are built around the gold core of the unknown cluster, with selective ranking of the most probable structures. Au: orange, S: yellow, carbon backbone in ligands: cyan.

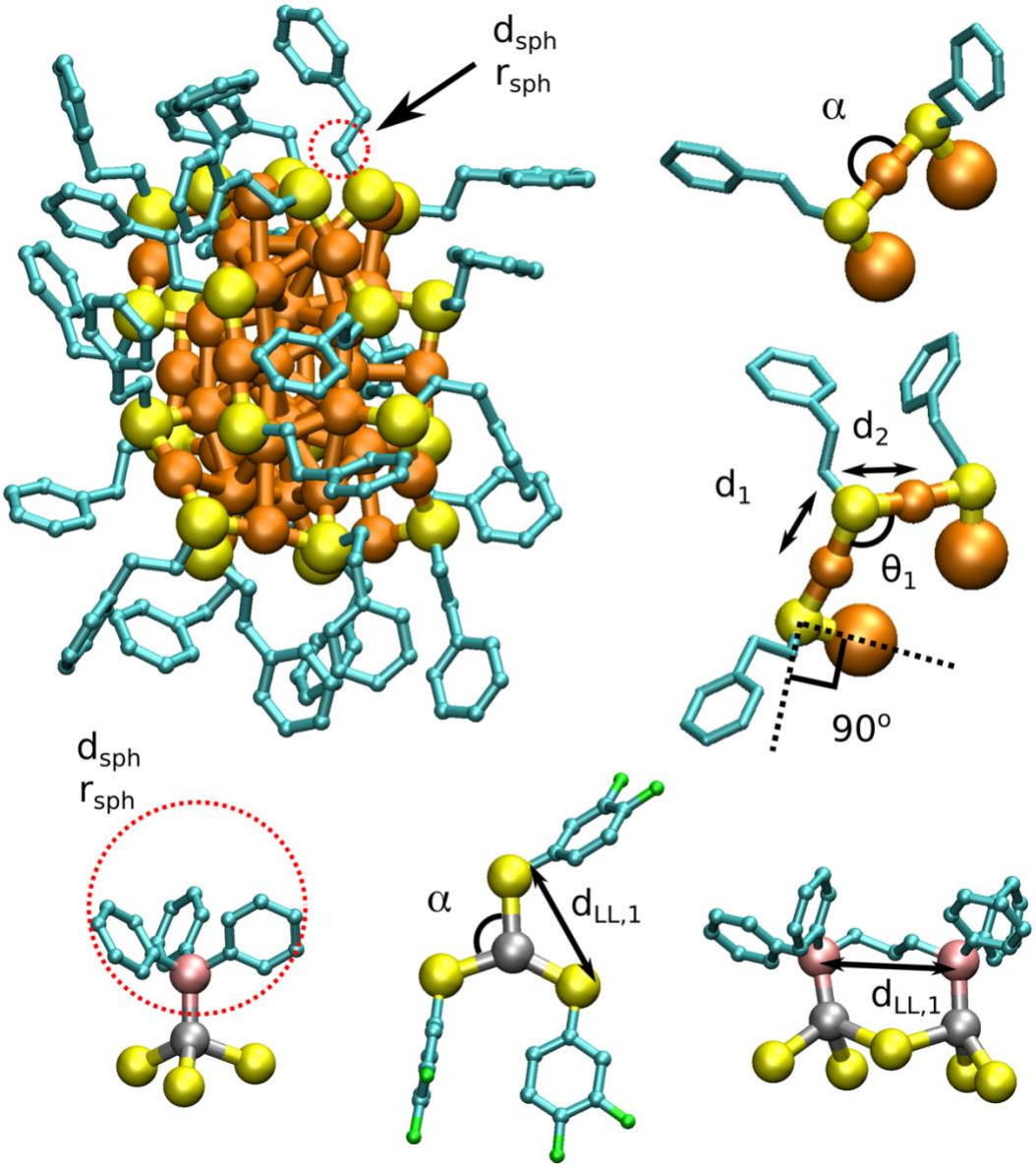

Figure 2 | Parameters related to the local environment of S-atoms. d_1 and d_2 are the two nearest neighbour Au-S distances and θ_1 is the selected bond angle between S-atom and the two nearest neighbour Au-atoms. Criteria for the S-Au-S and S-Ag-S bond angles (α) close to 180 degrees are used for adding or recognizing the atoms in a linear SR-Au-SR and SR-Ag-SR conformations and 120 degrees for three-coordinated Ag-S complexes. Spatial fitting of ligands is tested with a rigid sphere (red dashed circles) in a perpendicular direction to the two nearest neighbor Au-S bonds of each S-atom and parallel to Au-P bond for phosphines. Distance of the sphere from the binding site S-atom is also defined. Here, the sphere mimicks the first CH_2 group of phenyl ethane thiol SCH_2CH_2Ph and the whole Ph_3 group for PPh_3 ligand. $d_{LL,1}$ represents the distances between of the added interface atoms which are restricted by parameters when adding special local structures or when limiting the smallest possible interface atom distances. Colors: Ag: gray, F: green, P: pink and the rest as in Figure 1.

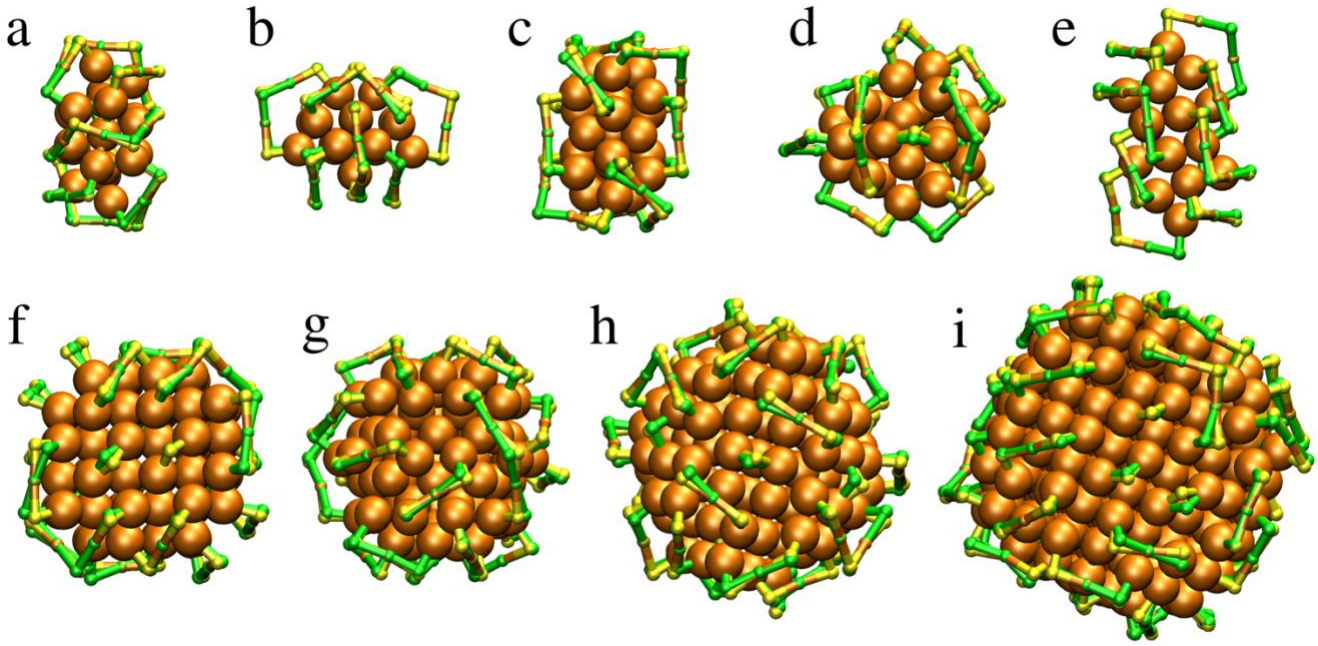

Figure 3 | Validation of structure prediction for Au-clusters. Comparison of the predicted and true ligand-metal interface structures of protected Au-clusters: **a** $Au_{34}(SR)_{22}$ (ref. 14), **b** $Au_{36}(SR)_{24}$ (ref. 15), **c** $Au_{38}(SR)_{24}$ (ref. 16), **d** $Au_{44}(SR)_{26}$ (ref. 17), **e** $Au_{52}(SR)_{32}$ (ref. 18), **f** $Au_{92}(SR)_{44}$ (ref. 19), **g** $Au_{102}(SR)_{44}$ (ref. 20), **h** $Au_{146}(SR)_{57}$ (ref. 21), and **i** $Au_{279}(SR)_{84}$ (ref. 22). Predicted S-atoms and Au-S bonds are drawn in green and true in yellow. Au-atoms are drawn with orange color.

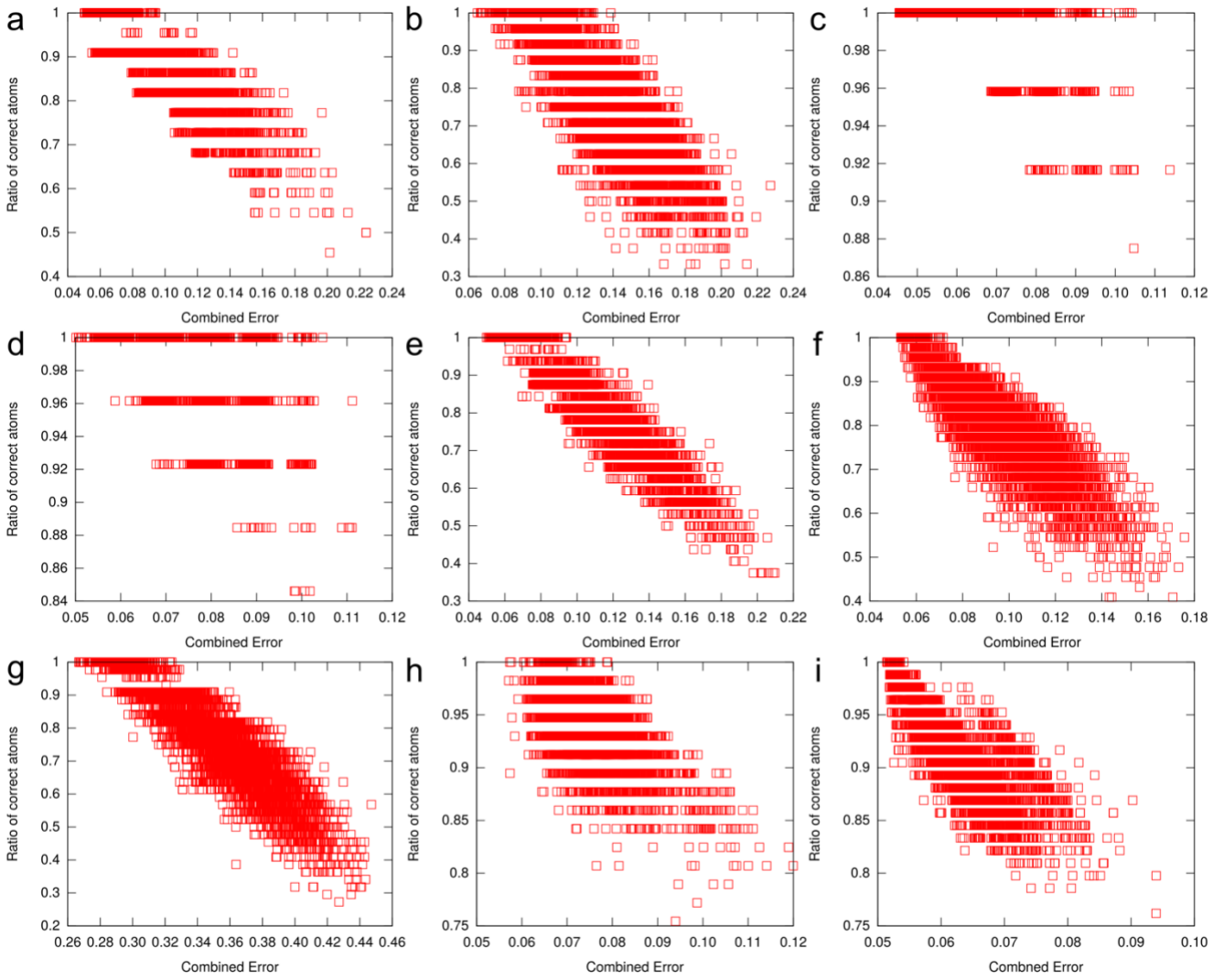

Figure 4 | Determination of the true structure of Au-clusters using CSE ranking. Ratio of the correctly predicted S-atoms as a function of CSE for ligand protected Au-clusters: **a** $Au_{34}(SR)_{22}$, **b** $Au_{36}(SR)_{24}$, **c** $Au_{38}(SR)_{24}$, **d** $Au_{44}(SR)_{26}$, **e** $Au_{52}(SR)_{32}$, **f** $Au_{92}(SR)_{44}$, **g** $Au_{102}(SR)_{44}$, **h** $Au_{146}(SR)_{57}$ and **i** $Au_{279}(SR)_{84}$. CSE includes contributions from error of local environments of Au and S atoms as well as from the number of predicted S atoms in units and in total.

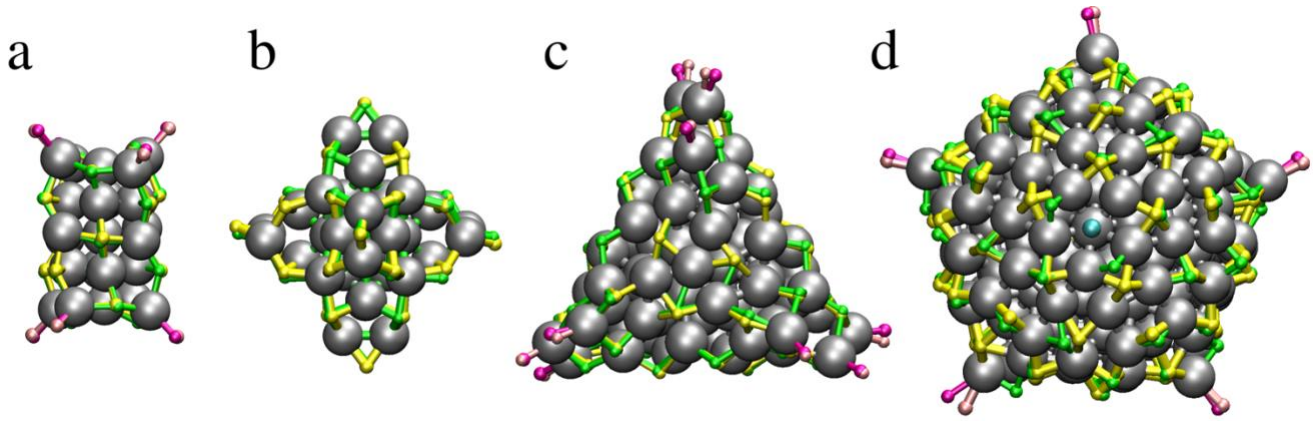

Figure 5 | Validation of structure prediction for Ag-clusters. Comparison of the predicted and true ligand-metal interface structures of protected Ag-clusters: **a** $Ag_{23}(SR)_{18}(PPh_3)_8$, **b** $Ag_{44}(SR)_{30}$, **c** $Ag_{78}(SR)_{42}(DPPP)_6$ and **d** $Ag_{211}Cl(SR)_{71}(PPh_3)_6$. tFor predicted clusters Ag-S bonds are drawn in green and true Ag-S bonds in yellow whereas Ag-P bonds are drawn in magenta for predicted structure and in pink for the true structure. In panel d) chlorine atom is drawn with light blue color.

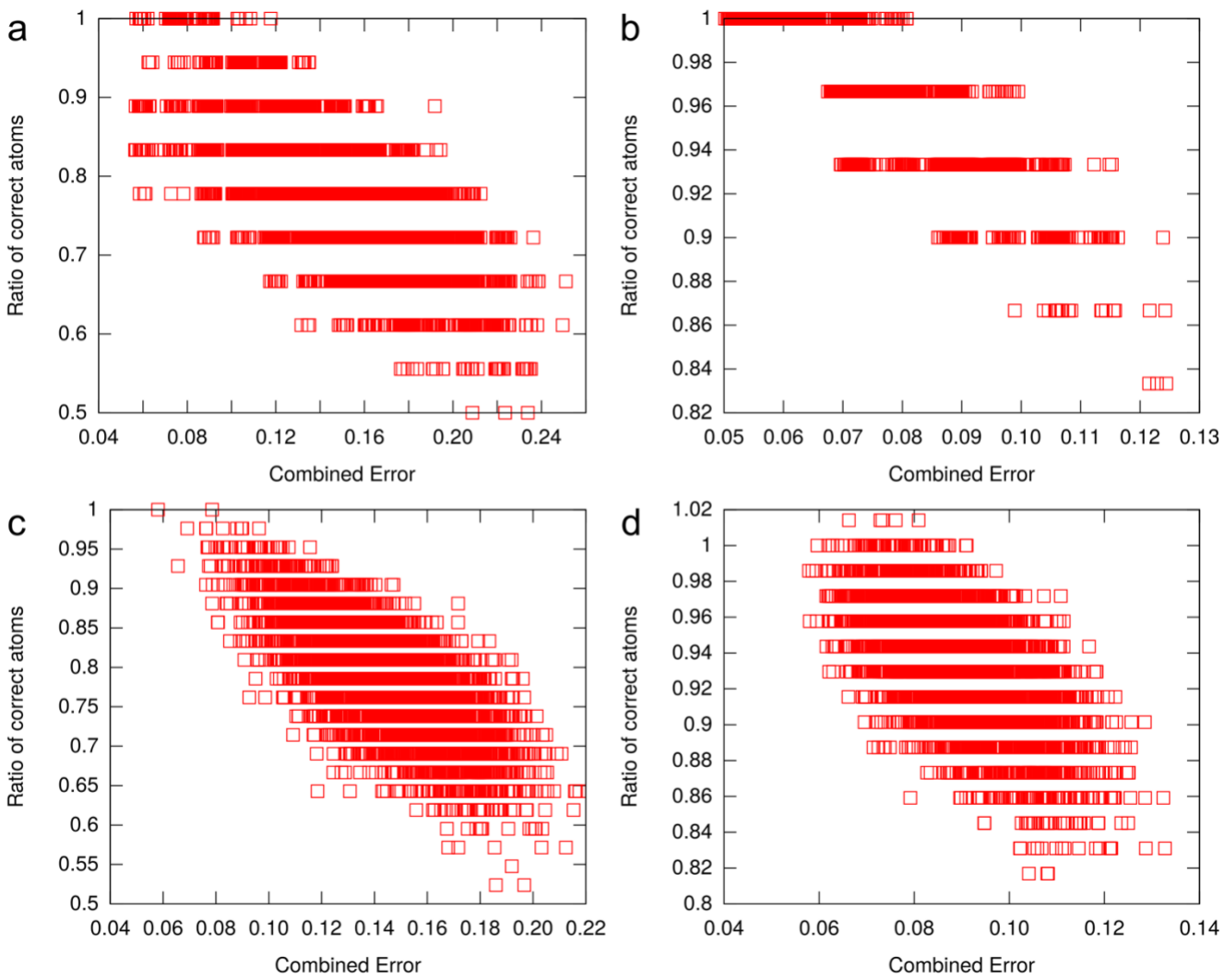

Figure 6 | Determination of the true structure of Ag-clusters using CSE ranking. Ratio of correctly predicted S-atoms as a function of CSE for ligand protected Ag-clusters: **a** $Ag_{23}(SR)_{18}(PPh_3)_8$, **b** $Ag_{44}(SR)_{30}$, **c** $Ag_{78}(SR)_{42}(DPPP)_6$ and **d** $Ag_{211}Cl(SR)_{71}(PPh_3)_6$. CSE includes contributions from error of local environments of Ag and S atoms as well as from the number of predicted S atoms in units and in total.

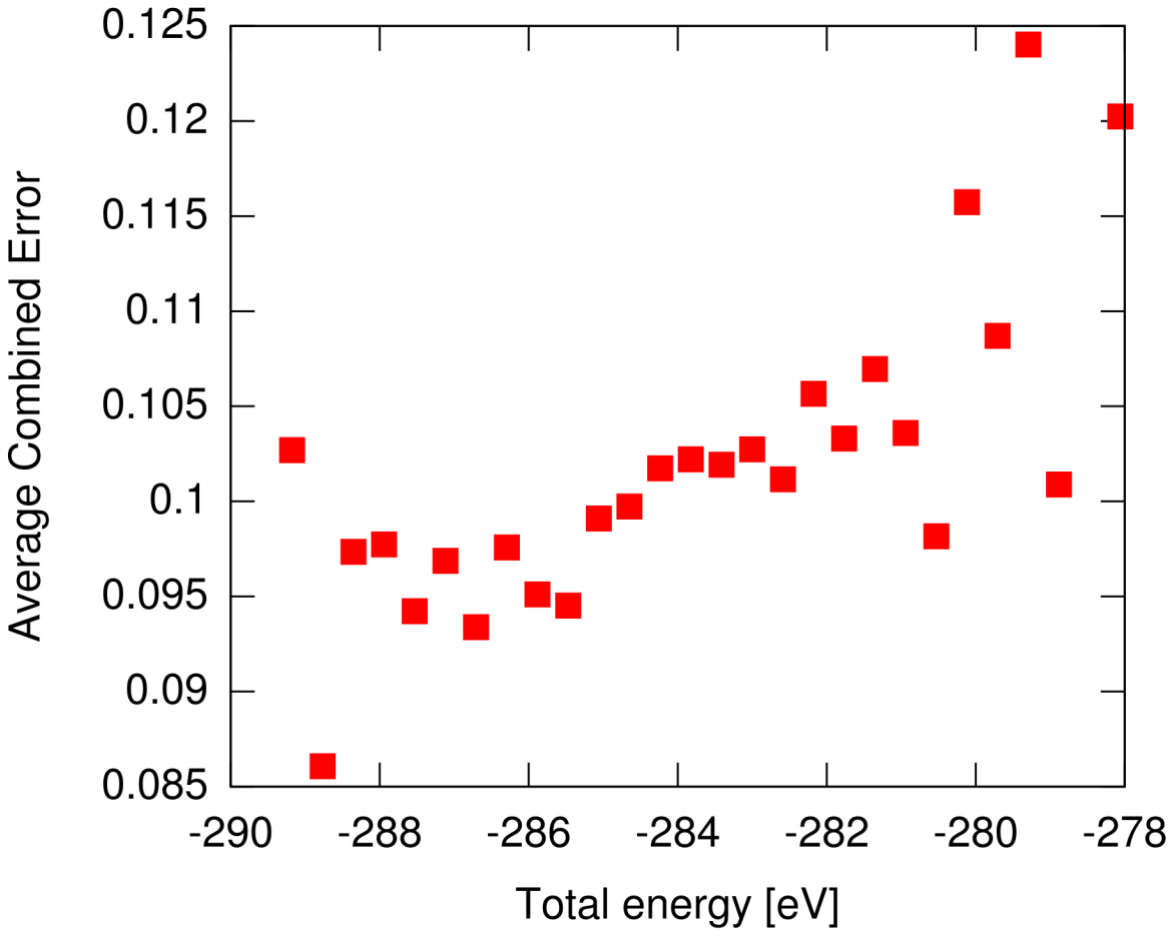

Figure 7 | CSE correlates with DFT total energy. CSE as a function of the DFT total energy of the model structures of $Au_{36}(SR)_{24}$ cluster. All the 700 model structures that have exactly 24 ligands were chosen for the analysis. CSE was calculated as an average over 0.4 eV energy range. For the calculation of the total energy, the SR-group is simplified with the SH-group.

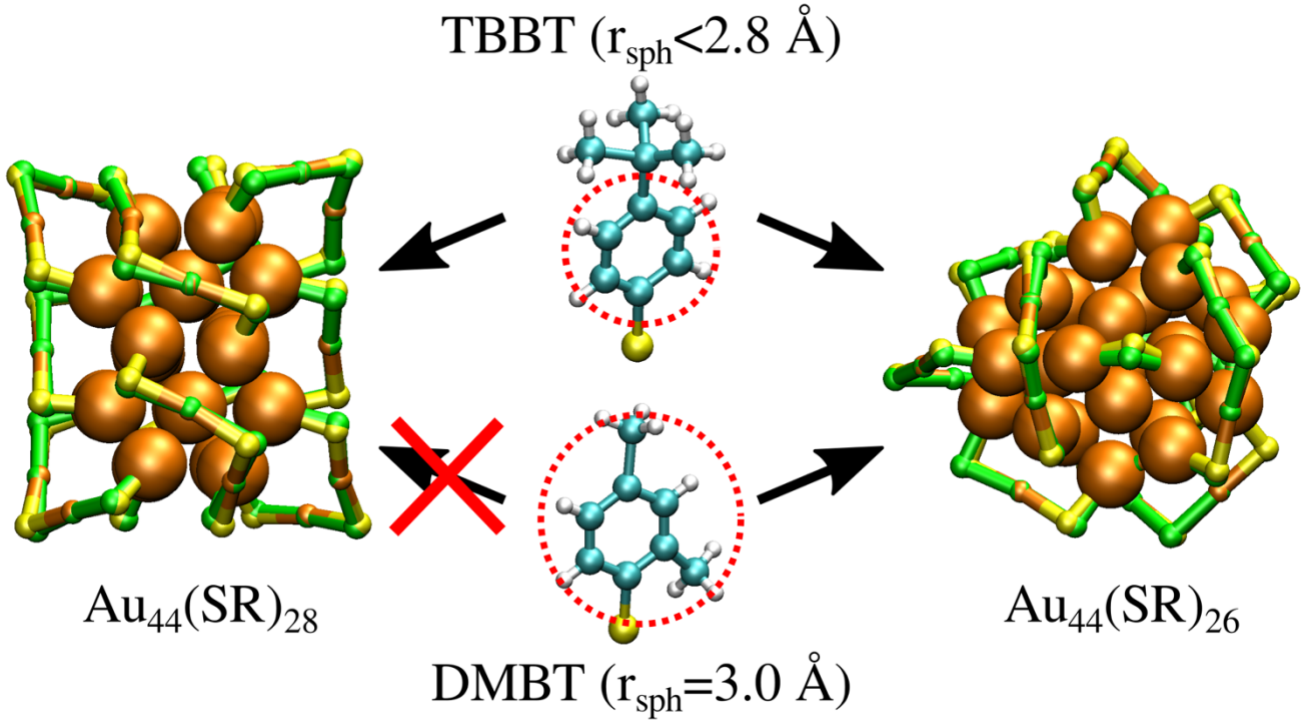

Figure 8 | Size of the ligands affects the structure. Predicted model structures of $Au_{44}(SR)_{26}$ and $Au_{44}(SR)_{28}$ clusters for different ligands. Due to spatial fitting of the organic part of the ligand $Au_{44}(SR)_{28}$ is found only for ligand sizes < 2.8 Å as mimicked by the spherical probe (see Supplementary Table 6). The maximum number of ligands with 3.0 Å probe on $Au_{44}(SR)_{28}$ surface is 26.

Table 1. The results of predicting sulfur positions for ligand-protected Au- and Ag-clusters.

Cluster	Number of model structures	Max in units $N_{max,unit}$	In total if max in units $N_{max,tot}$	Correct structures in % [(1)]	Min RMSD of correct structures [Å]
$Au_{34}(SR)_{22}$	9216	22	22	28.0 % (2579)	0.261
$Au_{36}(SR)_{24}$	9216	24	24	6.66% (614)	0.432
$Au_{38}(SR)_{24}$	9216	24	24	94.0% (8665)	0.383
$Au_{44}(SR)_{26}$	9216	24	25-26	85.2% (7853)	0.339
$Au_{52}(SR)_{32}$	9216	32	32	9.39 % (865)	0.319
$Au_{92}(SR)_{44}$	9216	36	39-44	1.79% (165)	0.525
$Au_{102}(SR)_{44}$	9216	44	44	5.41% (499)	0.395
$Au_{146}(SR)_{57}$	9216* [(2)]	50	54-60	1.21 % (121)	0.545
$Au_{279}(SR)_{84}$	9216*	60	75-84	0.67 % (62)	0.539
$Ag_{23}(SR)_{18}(PPh_3)_8$	9216	18	18	1.19 % (110)	0.225
$Ag_{44}(SR)_{30}$	9216	30	30	42.9 % (3958)	0.375
$Ag_{78}(SR)_{42}(DPPP)_6$	9216	40	41-42	0.022 % (2)	0.644
$Ag_{211}Cl(SR)_{71}(PPh_3)_6$	9216*	70	70-72	0.85 % (78)	0.744

[(1)] In the case of Au clusters, the criterion to have the "correct structure" is that 2/2 of nn are correct for each atom. In the care of Ag clusters, the criterion is 4/5 of nn to be correct for each atom.
[(2)] Iterative prediction runs.

Supplementary Information

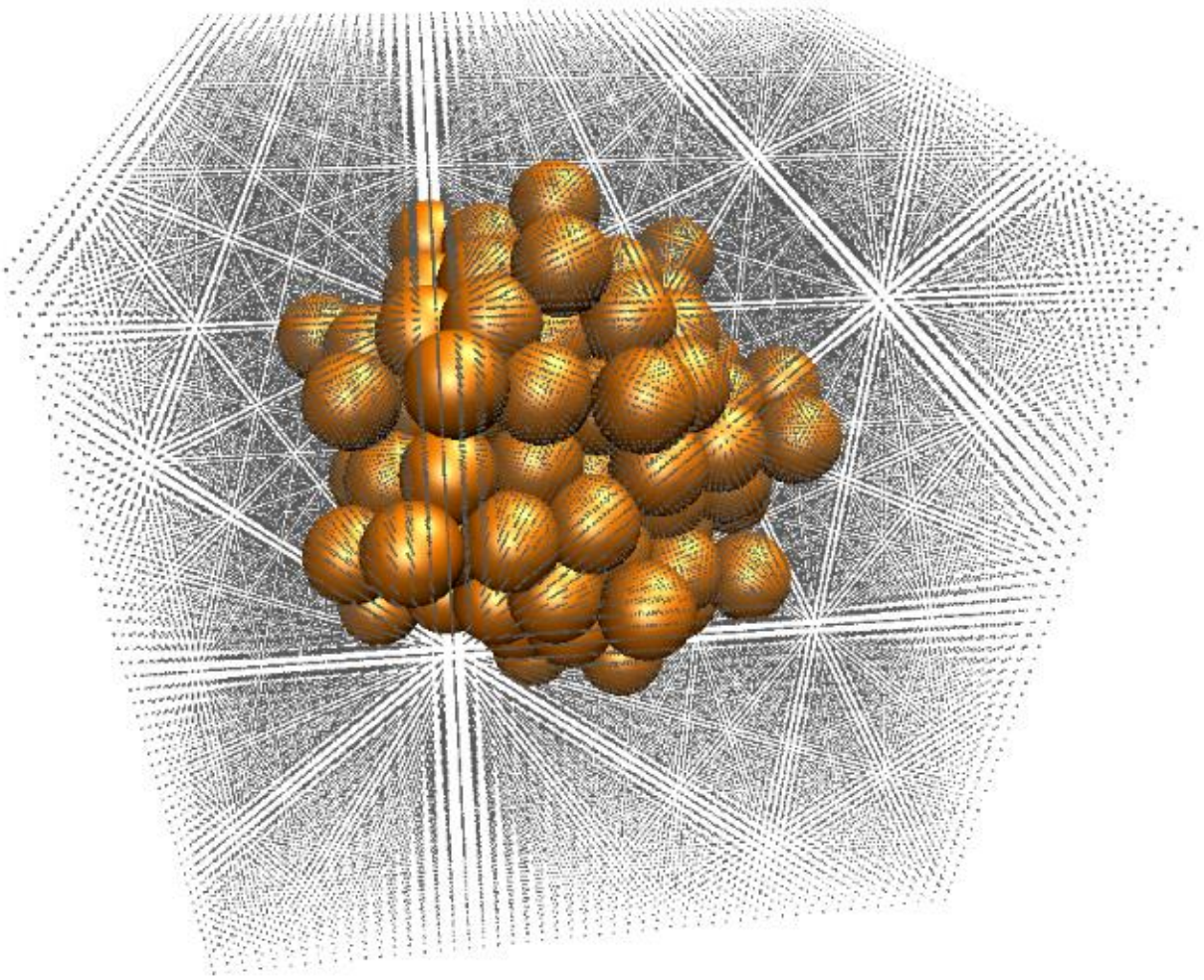

Supplementary Figure 1. Visualization of a 3D grid centered around the gold atoms of a $Au_x(SR)_y$ cluster. Possible sites for sulfur atoms at the gold surface are tested at the grid points using criteria based on the reference structures of known $Au_x(SR)_y$ clusters. In this work, the interval between grid points was 0.2 Å in all directions.

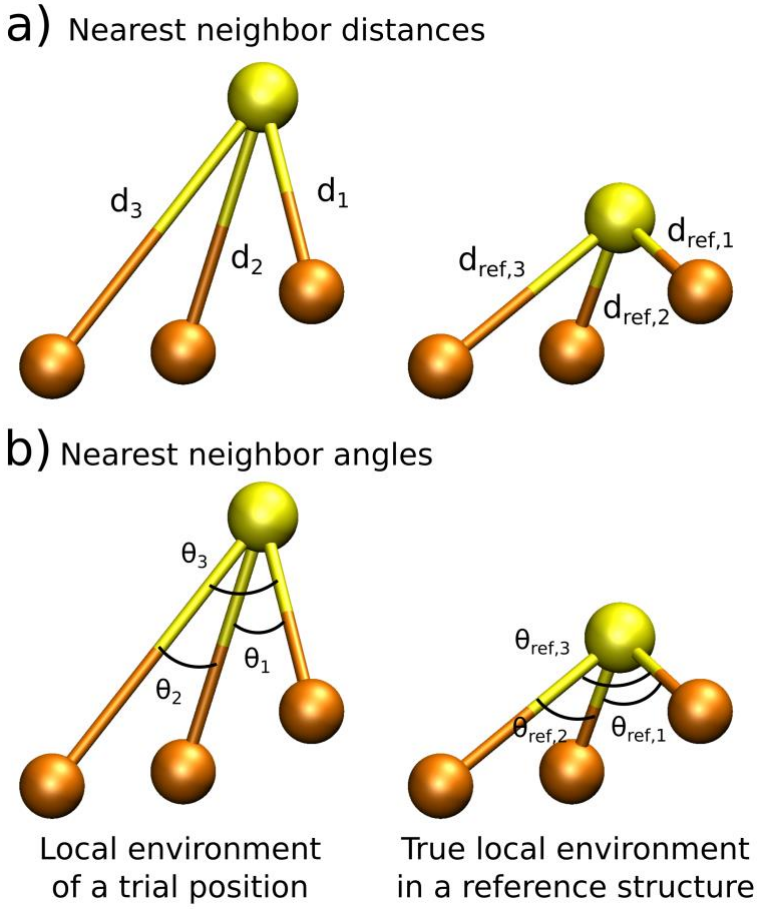

Supplementary Figure 2. An example of three nearest neighbour distances (a) and angles (b) for a trial grid point on the left and for a true S-atom of a reference structure on the right defining the local environment of a S-atom (yellow) with respect to Au-atoms (orange). A match in the selected bond distances and angles is one criterion to accept a grid point (Supplementary Fig.1) as a possible S-atom position. All possible angles between the nearest neighbor atoms to the grid point are tested.

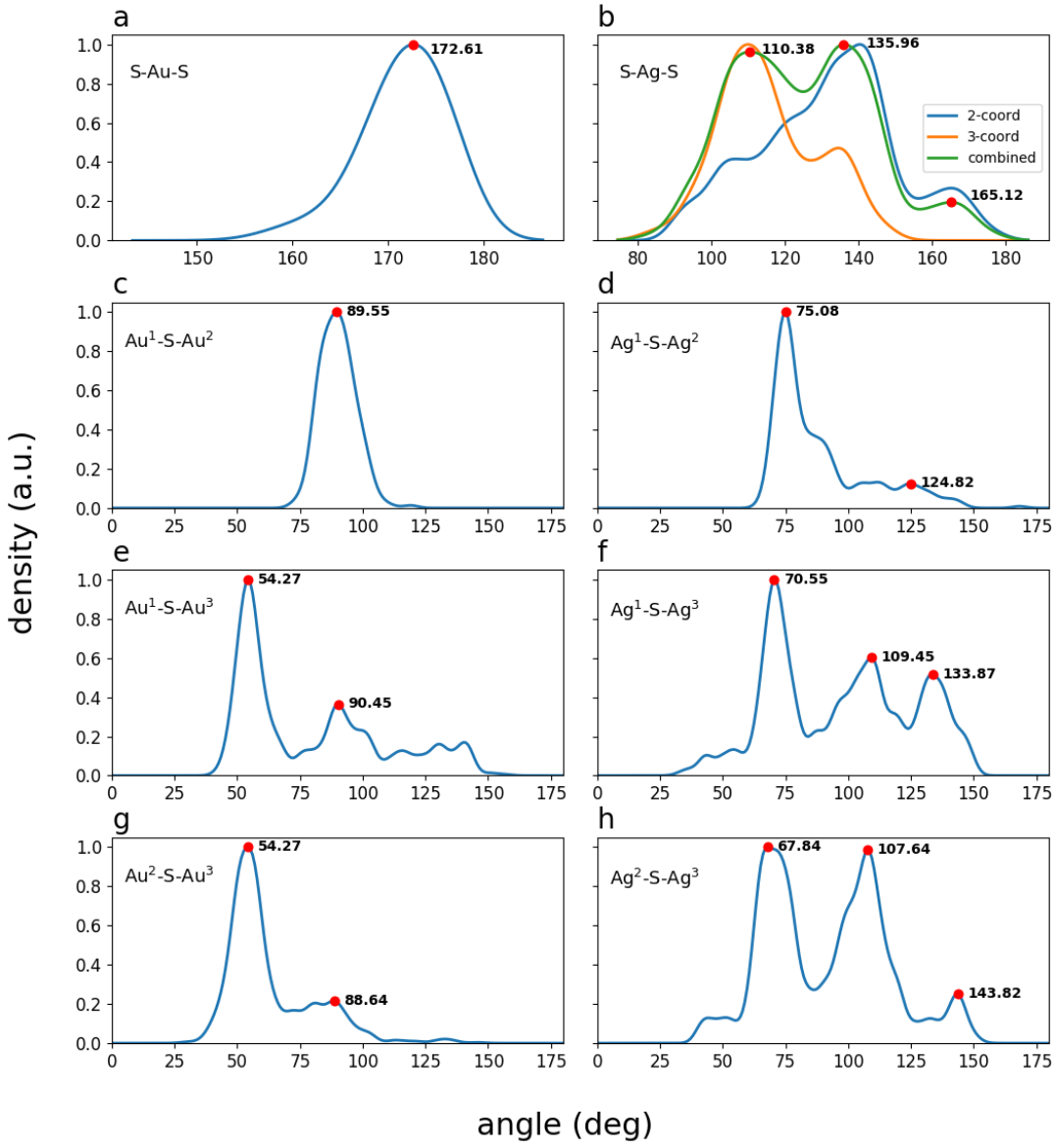

Supplementary Figure 3: Statistics of the nearest neighbor bond angles centered on gold (a), silver (b) and sulfur atoms (c-h) collected the reference structures listed in Supplementary Material. a) The angle formed by S-Au-S configuration is focused close to the 180, ideal in the linear SR-Au-SR conformations. b) the angles formed by S-Ag-S configuration are located close to 180 but also around 120, because of the coordination of silver atom. Major angles are formed tetrahedral-like 3-coordinated silver, triangle-shaped 2-coordinated configuration and almost straight 2-coordinated configuration. c) - h) all nearest neighbor bond angles that can be formed between the sulfur and its three nearest neighbor Au-atoms or Ag-atoms. Superscripts corresponds to the nearest neighbor order. All densities are calculated using gaussian spreading.

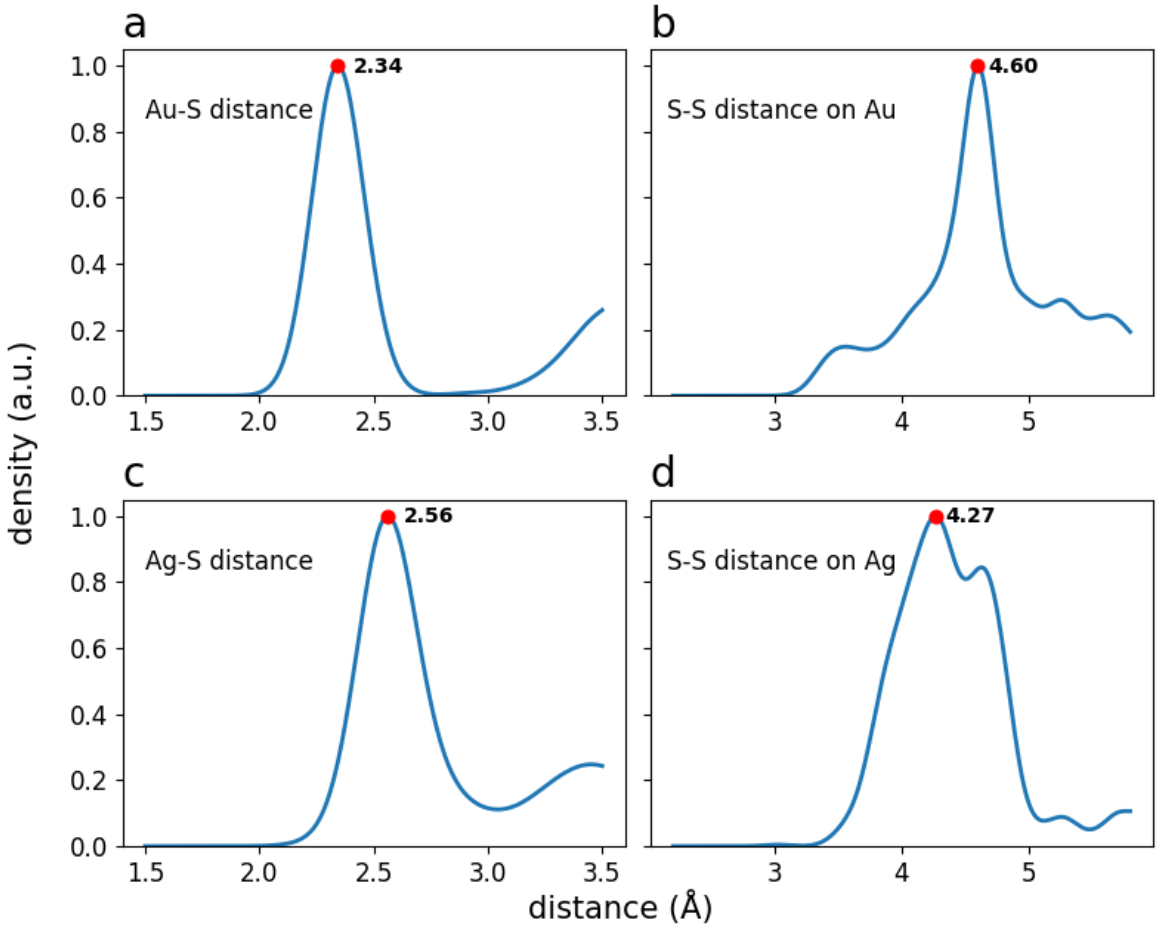

Supplementary Figure 4: Statistics from the atomic distances measured between the metal atoms and the sulfur atoms and between the sulfur atoms from all reference structures in following order: a) distance between gold and sulfur atoms, b) distance between sulfur atoms on gold clusters, c) distance between silver and sulfur atoms, d) distance between sulfur atoms on silver clusters. All densities are calculated using gaussian spreading.

Supplementary Table 1: Parameters for predicting thiol positions on the surface of the studied ligand protected Au-clusters.

Cluster	Ligand SR / R'	Local environments nd / Δd / Δθ	Protecting units α1 / Δα	Ligand fitting dsph / rsph	Min S to S distances [Å] dLL,1 / dLL,2
Au34(SR)22	SC6H11 / C6H11	3 / 0.1 / 10	175 / 5	3.2 / 2.5	3.0 / 3.5
Au36(SR)24	TBBT / Ph	3 / 0.2 / 10	175 / 5	3.2 / 2.5	3.0 / 3.5
Au38(SR)24	PET / CH2	3 / 0.1 / 10	175 / 5	1.8 / 2.1	3.0 / 3.5
Au44(SR)26	2,4-DMBT / DMBT	3 / 0.1 / 10	175 / 5	3.2 / 3.0	3.0 / 3.5
Au52(SR)32	PET / CH2	3 / 0.1 / 10	175 / 5	1.8 / 2.1	3.0 / 3.5
Au92(SR)44	TBBT / Ph	3 / 0.1 / 10	175 / 5	3.2 / 2.5	3.0 / 3.5
Au102(SR)44	pMBA / Ph	3 / 0.2 / 15	175 / 5	3.2 / 2.5	3.0 / 3.5
Au146(SR)57	pMBA / Ph	4 / 0.3 / 20	175 / 5	3.2 / 2.5	3.0 / 3.5
Au279(SR)84	TBBT / Ph	3 / 0.1 / 10	175 / 5	3.2 / 2.5	3.0 / 3.5

Supplementary Table 2: Parameters for predicting sulfur positions on the surface of studied ligand protected Ag-clusters.

Cluster	Ligands SR / R'	Local environments nd / Δd / Δθ	Protecting units α1 / α2 / Δα	Ligand fitting dsph / rsph	Min S to S distances [Å] dLL,1 / dLL,2
Ag23(SR)18(PPh3)8	PET / CH2	3 / 0.1 / 10	120 / 170 / 5	1.8 / 2.1	3.5 /3.5
Ag44(SR)30	SPhF2 / Ph	4 / 0.2 / 15	120 / 170 / 5	3.2 / 2.5	3.5 /3.5
Ag78(SR)42(DPPP)6	SPhCF3 / Ph	3 / 0.1 / 10	120 / 170 / 5	3.2 / 2.5	3.5 /3.5
Ag211Cl(SR)71(PPh3)6	SPhiPr / Ph	3 / 0.1 / 10	120 / 170 / 5	3.2 / 2.5	3.5 /3.5

Supplementary Table 3: Parameters for predicting phosphine and diphosphine positions for ligand protected Ag-clusters. Predictions are made starting with a initial model structure after the prediction of sulfur positions (see in Tables 1 and 2).

Cluster	Phosphine ligand	Local environments nd / Δd / Δθ	P to P distances in diphosphines ddiP	Ligand fitting dsph / rsph	Min P to P distances [Å] dLL,1 / dLL,2
Ag23(SR)18(PPh3)8	PPh3	4 / 0.1 / 10	-	3.4 / 4.6	- / 3.5
Ag78(SR)42(DPPP)6	DPPP	4 / 0.2 / 10	5.0 – 5.5	3.4 / 4.6	3.5 / 3.5
Ag211Cl(SR)71(PPh3)6	PPh3	4 / 0.2 / 10	-	3.4 / 4.6	- / 3.5

Supplementary Table 4. The results of predicting phosphine and diphosphine positions (PPh_3 or DPPP) for ligand protected Ag-clusters.

Cluster	Number of model structures	Max in tot	Correct structures % 4/5 of nn correct for each atom	Min RMSD of correct structures [Å]
$Ag_{23}(SR)_{18}(PPh_3)_8$	3072	8	100% (3072)	0.266
$Ag_{78}(SR)_{42}(DPPP)_6$	3072	6	100% (3072)	0.480
$Ag_{211}Cl(SR)_{71}(PPh3)_6$	3072	6	100% (3072)	0.633

Supplementary Table 5: Parameters of predicting sulfur atom positions Au44(SR)26 and Au44(SR)28 using different size of spherical probes for ligands.

Cluster	Ligand SR	Local environments nd / Δd / Δθ	Protecting units α1 / Δα	Ligand fitting dsph / rsph	Min S to S distances [Å] dLL,1 / dLL,2
Au44(SR)26	2,4-DMBT	3 / 0.1 / 10	175 / 5	3.2 / **3.0**	3.0 / 3.5
Au44(SR)28	TBBT	3 / 0.2 / 10	175 / 5	3.2 / **2.8**	3.0 / 3.5
Au44(SR)28	TBBT	3 / 0.1 / 10	175 / 5	3.2 / **3.0**	3.0 / 3.5

Supplementary Table 6. The results of predicting sulfur positions for $Au_{44}(SR)_{28}$ using different size of spherical probes for ligand fitting as compared to $Au_{44}(SR)_{26}$ cluster.

Cluster	Number of model structures	Ligand SR	Ligand fitting dsph / rsph	Max in units	In total if max in units	Correct structures in % 2/2 of nn correct for each atom
$Au_{44}(SR)_{26}$	9216	2,4-DMBT	3.2 / 3.0	24	25-26	28.0 % (2579)
$Au_{44}(SR)_{28}$	9216	TBBT	3.2 / 2.8	28	28	5.90 % (544)
$Au_{44}(SR)_{28}$	9216	TBBT	3.2 / 3.0	24	26	0.00 % (0)

Supplementary Note 1: Combined structural error (CSE)

CSE is calculated from four different contributions: bond distances, bond angles, number of interface atoms in special local conformations, number of interface atoms in total. The error is calculated from all contributions as a relative number (percentages from the expected values) without special units.

$$\text{Combined Structural Error} = \frac{1}{4}[\Delta nn + \Delta N_{unit} + \Delta N_{tot}]$$

$$\Delta N_{unit} = \frac{|N_{unit} - N_{max,unit}|}{N_{max,unit}}$$

$$\Delta N_{tot} = \frac{|N_{tot} - N_{max,tot}|}{N_{max,tot}}$$

where $N_{max,tot}$ is defined from the set of generated model structures having maximum number, $N_{max,unit}$, of interface atoms in special local structure conformations (like protecting units). N_{unit} and N_{tot} are the number of interface atoms in special local conformations and in total respectively for the model structure in question.

$$\Delta nn = \frac{1}{N}\sum_{i=1}^{N} \; min_j[\Delta d_{ij} + \Delta\theta_{ij}]$$

$$\Delta d_{ij} = \frac{1}{n_d}\sum_{m=1}^{n_d} \frac{|d_m^i - d_m^{j,ref}|}{d_m^{j,ref}}$$

$$\Delta\theta_{ij} = \frac{1}{n_\theta}\sum_{m=1}^{n_\theta} \frac{|\theta_m^i - \theta_m^{j,ref}|}{\theta_m^{j,ref}}$$

where d_m^i and θ_m^i refer to mth nn-bond distance and angle for a model structure atom i and $d_m^{j,ref}$ and $\theta_m^{j,ref}$ to mth nn-bond distance and angle for a reference structure atom j. For all atoms the minimum average error in local environment of n_d nearest neigbor distances and n_θ nearest neighbor angles contributes in the combined structural error.
Minimization or the error contributions is done with respect to the known local environments of similar type of atoms j found in the set reference structures.

Supplementary Note 2: Approach for optimizing the process against stochastic challenges.

To overcome the challenges of the non-guided stochastic process, we introduce one possible approach to optimize the structural search. In more complex systems with increasing number of possible metal-ligand interface conformations the structural search can be improved by repeating the algorithm multiple times. For each repetition, the set of possible interface atom positions should be constructed from interface atoms of the best model structures of previous run, ranked by criteria discussed later. In this study, we have used 20 best model structures for this purpose, which have the largest number of interface atoms in specified protecting motifs and in total.

Supplementary Note 3: Validation of selected parameters.

The algorithm is based on a restricted structural search in which the simple rules depict the crucial physical and chemical insights into the process. The reference structures define the chemistry in form of local environments of atoms when finding the plausible interface atom positions (Algorithm 2). The realistic interface atom positions are accepted based on the nearest neighbor bond distances and bond angles within prescribed error limits. In the algorithm these are parameterized and in this study 3-4 nearest neighbors with 0.1-0.3 Å error limits for individual bond distances and 10-20 degrees for individual bond angles is used. The selected error limits of the bond distances and bond angles reflect the statistics collected from the known reference structures of the same class as listed in the Supplementary Material. We analysed statistics from the nearest neighbor Au-S, Ag-S bond distances and from Au-S-Au and Ag-S-Ag bond angles which are shown in Supplementary Fig. 3. These parameters dictate how close the local environment of a trial position has to be to the known environments of reference structures in order to be accepted. As a general instruction for prediction of more complex systems, it is better to increase the number of nearest neighbors and loosen the error limits for the bonds and angles instead of decreasing the number of nearest neighbors and restricting the criteria. The same instruction is valid when the number of reference structures is low.

During the search of realistic interface atom positions in Algorithm 2, spatial fitting of the ligands is made with spherical probe in perpendicular direction to the two nearest neighbor Au-S and Ag-S bonds

for thiolates and parallel to the nearest neighbor Ag-P bond for phosphines (see Figure 2), which are the most natural bonding directions for the organic part of ligands in these systems. In addition to the bonding direction, the representative spherical probes have to be parameterized for the size and for the distance. The spherical probe should mimic the most important, rigid, molecular organic group closest to the binding site atom. In our study all the parameters are estimated based on the atomic distances.

From Supplementary Fig. 4 we can see that the nearest neighbor bond distributions have single maxima at 2.3-2.5 Å for both Au-S and Ag-S bonds. Broadening of the distribution confirms that all the nearest neighbor metal atoms of sulfur in protected Au- and Ag-clusters can be found within 1.95 – 2.75 Å, which is one the guiding lines used in structural search when nearest neighbor metal and interface atoms are defined in both Au- and Ag-clusters. Determining the covalently bound metal and interface atoms is important during the restricted model structure generation. By looking at the distributions of S-Au-S and S-Ag-S bond angles in Supplementary Fig. 3 it is realized that there exist some favorable local arrangements of metal and interface atoms. When model structures are generated, it is reasonable to try adding first the most favorable conformations for which Algorithm 3 concentrates on. In the protected Au-clusters, the linear SR-Au-SR conformations that form different length of SR-(Au-SR)n (N=1,2) protecting units, are in the majority. In protected Ag-clusters, the coordination of Ag-atoms to S-atoms is more flexible including also three-coordinated arrangements in addition to two-coordinated linear SR-Ag-SR conformations. From the analysis shown in Supplementary Fig. 3 we can see that the linear conformations create a maxima in Au-S-Au and Ag-S-Ag bond angles close to 180 degrees whereas for Ag-clusters there is lot of weight on angles around 120 degrees. These observations led us to define special local conformations based on relative angles between metal and interface atoms. In the first part, adding interface atoms only into such specific local structures will be allowed that have S-Au-S angles of 175 degrees and S-Ag-S angles of 120 and 170 degrees. At the same time, the maximum coordination of metal atoms to sulfur can be restricted to 2 for Au- and 3 for Ag-atoms (see Algorithm 4). For gold atoms, no three-coordinated conformations to sulfur are seen in the known thiolate protected clusters. For phosphines, the only special local structure that limits the prediction is related to diphosphines for which the distance between the individual P atoms is restricted by the length of the connecting organic molecular group. Hence, the P atoms are added in pairs within a restricted distance range.

During generation of the model structure it is important that the distances between the added interface atoms remain reasonable. Based on the analysis of the S to S distances on the surface of the known protected Au-clusters shown in Supplementary Fig. 4 we can see that the lower edge of the distance distribution is located at 3.0 Å in protected Au-clusters and at 3.5 Å in protected Ag-clusters. Because of that we restrict the minimum distance between added interface atoms to be at 3.0 Å for the S-atoms in linear S-Au-S conformations and at 3.5 Å for the bridged thiolates on Au-S interfaces. For Ag-S and Ag-P interfaces a minimum distance of 3.5 Å is used for all added interface atoms in all possible conformations. In true system ligands that are closer to the given limits have high probability to form a dimer and become detached from the surface in ambient conditions, hence, no S-S bonds are seen on the surface of the known protected Au- and Ag-clusters.

Supplementary Note 4:

Reference structures for protected Au-clusters

$Au_{18}(SC_6H_{11})_{14}$, **$Au_{20}(TBBT)_{16}$**, $Au_{21}(S\text{-}t\text{-}Bu)_{15}$, $Au_{21}(S\text{-}Adm)_{15}$, $[Au_{23}(SC_6H_{11})_{16}]^-$, $Au_{24}(S\text{-}Adm)_{16}$, $Au_{24}(SCH_2Ph\text{-}t\text{-}Bu)_{20}$, $Au_{25}(PET)_{18}$, $[Au_{25}(PET)_{18}]^+$, $[Au_{25}(PET)_{18}]^-$, $Au_{30}(S\text{-}Adm)_{18}$, $Au_{34}(SC_6H_{11})_{22}$, $Au_{36}(S\text{-}t\text{-}Bu)_{24}$, $[Au_{38}(PET)_{24}]_Q$, $[Au_{38}(PET)_{24}]_T$, $Au_{42}(SC_6H_{11})_{26}$, $Au_{44}(TBBT)_{28}$, $Au_{52}(TBBT)_{32}$, $Au_{92}(TBBT)_{44}$, $Au_{102}(p\text{-}MBA)_{44}$, $Au_{102}(p\text{-}MBA)_{43}(p\text{-}BBT)$, $Au_{130}(p\text{-}MBT)_{50}$, $Au_{133}(SPh\text{-}t\text{-}Bu)_{52}$, **$Au_{144}(SCH_2Ph)_{60}$**, $Au_{146}(p\text{-}MBA)_{57}$, $Au_{246}(p\text{-}MBT)_{80}$, $Au_{279}(SH)_{84}$
Originally structure was $Au_{279}(SPh\text{-}t\text{-}Bu)_{84}$ but cif does not include ligands.

Structures that are used in actual algorithm but not in statistics are **bolded**.

In contrary to all other studied Au-clusters, the short and the long unit structures shown in Supplementary Figure 3 were used as reference structures for predicting the structure of $Au_{102}(SR)_{44}$ cluster.

Reference structures for protected Ag-clusters

$Ag_{14}(SPhF_2)_{12}(PPh_3)_8$, $Ag_{16}(DPPE)_4(SPhF_2)_{14}$, $Ag_{23}(PPh_3)_8(PET)_{18}$, $[Ag_{25}(SPhMe_2)_{18}]^-$, **$Ag_{29}(BDT)_{12}(PPh_3)_4$**, $[Ag_{32}(DPPE)_5(SC_6H_4CF_3)_{24}]^{2-}$, $Ag_{38}(SPhF_2)_{26}(P(C_4H_9)_3)_8$, $Ag_{38}(SPhF_2)_{26}(PPh_3)_8$, $[Ag_{44}(SPhF_2)_{30}]^{4-}$, $[Ag_{44}(SPhF)_{30}]^{4-}$, $[Ag_{45}(Dppm)_4(S\text{-}t\text{-}Bu)_{16}Br_{12}]^3$, $Ag_{50}(Dppm)_6(SCH_2Ph\text{-}t\text{-}Bu)_{30}$, $Ag_{63}(SPhF_2)_{36}(P(C_5H_{11})(C_4H_9)_2)_6(P(C_4H_9)_3)_2$, **$Ag_{78}(DPPP)_6(SPhCF_3)_{42}$**, $[Ag_{136}(SPh\text{-}t\text{-}Bu)_{64}Cl_3]^-$, $[Ag_{141}(S\text{-}Adm)_{40}Br_{12}]^{3+}$, $Ag_{210}(SPh\ ^iPr)_{71}(PPh_3)_5$, $Ag_{211}(SPh\ ^iPr)_{71}(PPh_3)_6$, $Ag_{374}(SPh\text{-}t\text{-}Bu)_{115}Br_2$

Structures that are used in actual algorithm but not in statistics are **bolded**.

References for the reference structures:

Au18:
Anindita Das, Chong Liu, Hee Young Byun, Katsuyuki Nobusada, Shuo Zhao, Nathaniel Rosi, Rongchao Jin. Structure Determination of [Au18(SR)14]. Angewandte Chemie, 2015, vol 54, iss. 10, pp 3140-3144, doi:10.1002/anie.201410161

Shuang Chen, Shuxin Wang, Juan Zhong, Yongbo Song, Jun Zhang, Hongting Sheng, Yong Pei, Manzhou Zhu. The Structure and Optical Properties of the [Au18(SR)14]. Nanocluster. Angewandte Chemie, 2015, vol. 54, iss. 10, pp 3145-3149, doi:10.1002/anie.201410295

Au20:
Chenjie Zeng, Chong Liu, Yuxiang Chen, Nathaniel L. Rosi, Rongchao Jin; Gold–Thiolate Ring as a Protecting Motif in the Au20(SR)16 Nanocluster and Implications, J. Am. Chem. Soc, 2014, vol. 136, iss. 34, pp 11922-11925, doi:10.1021/ja506802n

Au21 (t-bu):
Sha Yang, Jinsong Chai, Yongbo Song, Jiqiang Fan, Tao Chen, Shuxin Wang, Haizhu Yu, Xiaowu Li, Manzhou Zhu. In Situ Two-Phase Ligand Exchange: A New Method for the Synthesis of Alloy Nanoclusters with Precise Atomic Structures, J. Am. Chem. Soc., 2017, 139 (16), pp 5668–5671, DOI: 10.1021/jacs.7b00668

Au21 (Adm):
Shuang Chen, Lin Xiong, Shuxin Wang, Zhongyun Ma, Shan Jin, Hongting Sheng, Yong Pei, Manzhou Zhu. Total Structure Determination of Au21(S-Adm)15 and Geometrical/Electronic Structure Evolution of Thiolated Gold Nanoclusters, J. Am. Chem. Soc., 2016, 138 (34), pp 10754–10757, DOI: 10.1021/jacs.6b06004

Au23:
Anindita Das, Tao Li, Katsuyuki Nobusada, Chenjie Zeng, Nathaniel L. Rosi, Rongchao Jin. Nonsuperatomic [Au23(SC6H11)16]− Nanocluster Featuring Bipyramidal Au15 Kernel and Trimeric Au3(SR)4 Motif, J. Am. Chem. Soc., 2013, 135 (49), pp 18264–18267, DOI: 10.1021/ja409177s

Au24 (Adm):
David Crasto, Giovanni Barcaro, Mauro Stener, Luca Sementa, Alessandro Fortunelli, Amala Dass. Au24(SAdm)16 Nanomolecules: X-ray Crystal Structure, Theoretical Analysis, Adaptability of Adamantane Ligands to Form Au23(SAdm)16 and Au25(SAdm)16, and Its Relation to Au25(SR)18, J. Am. Chem. Soc., 2014, 136 (42), pp 14933–14940, DOI: 10.1021/ja507738e

Au24(SCH2Ph-t-Bu)20:
Anindita Das, Tao Li, Gao Li, Katsuyuki Nobusada, Chenjie Zeng, Nathaniel L. Rosi, Rongchao Jin. Crystal structure and electronic properties of a thiolate-protected Au24 nanocluster, Nanoscale, 2014, vol. 6, iss. 12, pp 6458-6462, DOI: 10.1039/C4NR01350F

Au25(-1):
Manzhou Zhu, Christine M. Aikens, Frederick J. Hollander, George C. Schatz Rongchao Jin. Correlating the Crystal Structure of A Thiol-Protected Au25 Cluster and Optical Properties, J. Am. Chem. Soc., 2008, 130 (18), pp 5883–5885, DOI: 10.1021/ja801173r

Michael W. Heaven, Amala Dass, Peter S. White, Kennedy M. Holt, Royce W. Murray. Crystal Structure of the Gold Nanoparticle [N(C8H17)4][Au25(SCH2CH2Ph)18], J. Am. Chem. Soc., 2008, 130 (12), pp 3754–3755
DOI: 10.1021/ja800561b

Au25(0):
Manzhou Zhu, William T. Eckenhoff, Tomislav Pintauer, Rongchao Jin. Conversion of Anionic [Au25(SCH2CH2Ph)18]− Cluster to Charge Neutral Cluster via Air Oxidation, J. Phys. Chem. C, 2008, 112 (37), pp 14221–14224, DOI: 10.1021/jp805786p

Au25(1):
Marcus A. Tofanelli, Kirsi Salorinne, Thomas W. Ni, Sami Malola, Brian Newell, Billy Phillips, Hannu Häkkinen, Christopher J. Ackerson. Jahn–Teller effects in Au25(SR)18, Chem. Sci., 2016, vol. 7, iss. 3, pp 1882-1890, DOI: 10.1039/C5SC02134K

Au30:
Tatsuya Higaki, Chong Liu, Chenjie Zeng, Renxi Jin, Yuxiang Chen, Nathaniel L. Rosi, Rongchao Jin. Controlling the Atomic Structure of Au30 Nanoclusters by a Ligand-Based Strategy, Angewandte Chemie, 2016, vol 55, iss. 23, pp 6694-6697, DOI: 10.1002/anie.201601947

Au34 and Au42:
Hongwei Dong, Lingwen Liao, Shengli Zhuang, Chuanhao Yao, Jishi Chen, Shubo Tian, Min Zhu, Xu Liu, Lingling Li, Zhikun Wu. A novel double-helical-kernel evolution pattern of gold nanoclusters: alternate single-stranded growth at both ends, Nanoscale, 2017, vol. 9, iss. 11, pp 3742-3746, DOI: 10.1039/C6NR09724C

Au38 Q:
Huifeng Qian, William T. Eckenhoff, Yan Zhu, Tomislav Pintauer, Rongchao Jin. Total Structure Determination of Thiolate-Protected Au38 Nanoparticles, J. Am. Chem. Soc., 2010, 132 (24), pp 8280–8281, DOI: 10.1021/ja103592z

Au38 T:
Shubo Tian, Yi-Zhi Li, Man-Bo Li, Jinyun Yuan, Jinlong Yang, Zhikun Wu, Rongchao Jin. Structural isomerism in gold nanoparticles revealed by X-ray crystallography. Nature Communications, 2015, volume 6, article number: 8667, DOI: 10.1038/ncomms9667

Au44:
Chenjie Zeng, Yuxiang Chen, Kenji Iida, Katsuyuki Nobusada, Kristin Kirschbaum, Kelly J. Lambright, Rongchao Jin. Gold Quantum Boxes: On the Periodicities and the Quantum Confinement in the Au28, Au36, Au44, and Au52 Magic Series, J. Am. Chem. Soc., 2016, 138 (12), pp 3950–3953, DOI: 10.1021/jacs.5b12747

Au52:
Shengli Zhuang, Lingwen Liao, Man-Bo Li, Chuanhao Yao, Yan Zhao, Hongwei Dong, Jin Li, Haiteng Deng, Lingling Li, Zhikun Wu. The fcc structure isomerization in gold nanoclusters, Nanoscale, 2017, vol. 9, iss. 39, pp 14809-14813, DOI: 10.1039/C7NR05239A

Au92:
Chenjie Zeng, Chong Liu, Yuxiang Chen, Nathaniel L. Rosi, Rongchao Jin, Atomic Structure of Self-Assembled Monolayer of Thiolates on a Tetragonal Au92 Nanocrystal, J. Am. Chem. Soc., 2016, 138 (28), pp 8710–8713, DOI: 10.1021/jacs.6b04835

Au102:
Pablo D. Jadzinsky, Guillermo Calero, Christopher J. Ackerson, David A. Bushnell, Roger D. Kornberg. Structure of a Thiol Monolayer-Protected Gold Nanoparticle at 1.1 Å Resolution, Science, 2007, Vol. 318, Issue 5849, pp. 430-433, DOI: 10.1126/science.1148624

Au102 (p-BBT):
Christine L. Heinecke, Thomas W. Ni, Sami Malola, Ville Mäkinen, O. Andrea Wong, Hannu Häkkinen, Christopher J. Ackerson. Structural and Theoretical Basis for Ligand Exchange on Thiolate Monolayer Protected Gold Nanoclusters, J. Am. Chem. Soc., 2012, 134 (32), pp 13316–13322, DOI: 10.1021/ja3032339

Au130:
Yuxiang Chen, Chenjie Zeng, Chong Liu, Kristin Kirschbaum, Chakicherla Gayathri, Roberto R. Gil, Nathaniel L. Rosi, Rongchao Jin. Crystal Structure of Barrel-Shaped Chiral Au130(p-MBT)50 Nanocluster, J. Am. Chem. Soc., 2015, 137 (32), pp 10076–10079, DOI: 10.1021/jacs.5b05378

Au133:
Chenjie Zeng, Yuxiang Chen, Kristin Kirschbaum, Kannatassen Appavoo, Matthew Y. Sfeir Rongchao Jin. Structural patterns at all scales in a nonmetallic chiral Au133(SR)52 nanoparticle, Science Advances, 2015, Vol. 1, no. 2, e1500045, DOI: 10.1126/sciadv.1500045

Au144:
Nan Yan, Nan Xia, Lingwen Liao, Min Zhu, Fengming Jin, Rongchao Jin, Zhikun Wu; Unraveling the long-pursued Au144 structure by x-ray crystallography, Science Advances, 2018, Vol. 4, no. 10, eaat7259, DOI: 10.1126/sciadv.aat7259

Au146:
Sandra Vergara, Dylan A. Lukes, Michael W. Martynowycz, Ulises Santiago, Germán Plascencia-Villa, Simon C. Weiss, M. Jason de la Cruz, David M. Black, Marcos M. Alvarez, Xochitl López-Lozano, Christopher O. Barnes, Guowu Lin, Hans-Christian Weissker, Robert L. Whetten, Tamir Gonen, Miguel Jose Yacaman, Guillermo Calero. MicroED Structure of Au146(p-MBA)57 at Subatomic Resolution Reveals a Twinned FCC Cluster, J. Phys. Chem. Lett., 2017, 8 (22), pp 5523–5530, DOI: 10.1021/acs.jpclett.7b02621

Au246:
Chenjie Zeng, Yuxiang Chen, Kristin Kirschbaum, Kelly J. Lambright, Rongchao Jin. Emergence of hierarchical structural complexities in nanoparticles and their assembly, Science, 2016, Vol. 354, Issue 6319, pp. 1580-1584, DOI: 10.1126/science.aak9750

Au279:
Naga Arjun Sakthivel, Shevanuja Theivendran, Vigneshraja Ganeshraj, Allen G. Oliver, Amala Dass. Crystal Structure of Faradaurate-279: Au279(SPh-tBu)84 Plasmonic Nanocrystal Molecules, J. Am. Chem. Soc., 2017, 139 (43), pp 15450–15459, DOI: 10.1021/jacs.7b08651

Ag14:
Huayan Yang, Jing Lei, Binghui Wu, Yu Wang, Meng Zhou, Andong Xia, Lansun Zheng, Nanfeng Zheng. Crystal structure of a luminescent thiolated Ag nanocluster with an octahedral Ag64+ core, Chem. Commun., 2013, vol. 49, iss. 3, pp 300-302, DOI: 10.1039/C2CC37347E

Ag16 & Ag32:
Huayan Yang, Yu Wang, Nanfeng Zheng. Stabilizing subnanometer Ag(0) nanoclusters by thiolate and diphosphine ligands and their crystal structures, Nanoscale, 2013, vol. 5, iss. 7, pp 2674-2677, DOI: 10.1039/C3NR34328F

Ag23:
Chao Liu, Tao Li, Hadi Abroshan, Zhimin Li, Chen Zhang, Hyung J. Kim, Gao Li, Rongchao Jin. Chiral Ag23 nanocluster with open shell electronic structure and helical face-centered cubic framework, Nature Communications, volume 9, Article number: 744 (2018), DOI: 10.1038/s41467-018-03136-9

Ag25:
Chakra P. Joshi, Megalamane S. Bootharaju, Mohammad J. Alhilaly, Osman M. Bakr. [Ag25(SR)18]−: The "Golden" Silver Nanoparticle, J. Am. Chem. Soc., 2015, 137 (36), pp 11578–11581, DOI: 10.1021/jacs.5b07088

Ag29:
Lina G. AbdulHalim, Megalamane S. Bootharaju, Qing Tang, Silvano Del Gobbo, Rasha G. AbdulHalim, Mohamed Eddaoudi, De-en Jiang, Osman M. Bakr; Ag29(BDT)12(TPP)4: A Tetravalent Nanocluster, J. Am. Chem. Soc. 2015, vol. 137, iss. 37, pp. 11970-11975, doi:10.1021/jacs.5b04547

Ag38 PC4 & Ag38 PPh3 & Ag63:
Huayan Yang, Juanzhu Yan, Yu Wang, Haifeng Su, Lars Gell, Xiaojing Zhao, Chaofa Xu, Boon K. Teo, Hannu Häkkinen, Nanfeng Zheng. Embryonic Growth of Face-Center-Cubic Silver Nanoclusters Shaped in Nearly Perfect Half-Cubes and Cubes, J. Am. Chem. Soc., 2017, 139 (1), pp 31–34, DOI: 10.1021/jacs.6b10053

Ag44 (F2) & Ag44 (F):
Huayan Yang, Yu Wang, Huaqi Huang, Lars Gell, Lauri Lehtovaara, Sami Malola, Hannu Häkkinen, Nanfeng Zheng. All-thiol-stabilized Ag44 and Au12Ag32 nanoparticles with single-crystal structures, Nature Communications, volume 4, Article number: 2422 (2013), DOI: 10.1038/ncomms3422

Ag44(SR)26:
Lingwen Liao, Shengli Zhuang, Chuanhao Yao, Nan Yan, Jishi Chen, Chengming Wang, Nan Xia, Xu Liu, Man-Bo Li, Lingling Li, Xiaoli Bao, Zhikun Wu; Structure of Chiral Au44(2,4-DMBT)26 Nanocluster with an 18-Electron Shell Closure, J. Am. Chem. Soc., 2016, vol. 138, iss. 33, doi: 10.1021/jacs.6b07178

Ag45:
Xuejuan Zou, Shan Jin, Wenjun Du, Yangfeng Li, Peng Li, Shuxin Wang, Manzhou Zhu. Multi-ligand-directed synthesis of chiral silver nanoclusters. Nanoscale, 2017, vol. 9, iss. 43, pp 16800-16805, DOI: 10.1039/C7NR06338E

Ag50:
Wenjun Du, Shan Jin, Lin Xiong, Man Chen, Jun Zhang, Xuejuan Zou, Yong Pei, Shuxin Wang, Manzhou Zhu. Ag50(Dppm)6(SR)30 and Its Homologue AuxAg50–x(Dppm)6(SR)30 Alloy Nanocluster: Seeded Growth, Structure Determination, and Differences in Properties, J. Am. Chem. Soc., 2017, 139 (4), pp 1618–1624, DOI: 10.1021/jacs.6b11681

Ag78:
Huayan Yang, Juanzhu Yan, Yu Wang, Guocheng Deng, Haifeng Su, Xiaojing Zhao, Chaofa Xu, Boon K. Teo, Nanfeng Zheng; From Racemic Metal Nanoparticles to Optically Pure Enantiomers in One Pot, J. Am. Chem. Soc., 2017, vol. 139, iss. 45, pp. 16113-16116, doi: 10.1021/jacs.7b10448

Ag136 & Ag374:
Huayan Yang, Yu Wang, Xi Chen, Xiaojing Zhao, Lin Gu, Huaqi Huang, Juanzhu Yan, Chaofa Xu, Gang Li, Junchao Wu, Alison J. Edwards, Birger Dittrich, Zichao Tang, Dongdong Wang, Lauri Lehtovaara, Hannu Häkkinen, Nanfeng Zheng. Plasmonic twinned silver nanoparticles with molecular precision, Nature Communications volume 7, Article number: 12809 (2016), DOI: 10.1038/ncomms12809

Ag141:
Liting Ren, Peng Yuan, Haifeng Su, Sami Malola, Shuichao Lin, Zichao Tang, Boon K. Teo, Hannu Häkkinen, Lansun Zheng, Nanfeng Zheng. Bulky Surface Ligands Promote Surface Reactivities of [Ag141X12(S-Adm)40]3+ (X = Cl, Br, I) Nanoclusters: Models for Multiple-Twinned Nanoparticles, J. Am. Chem. Soc., 2017, 139 (38), pp 13288–13291, DOI: 10.1021/jacs.7b07926

Ag210 & Ag211:
Jun-Yan Liu, Fahri Alkan, Zhi Wang, Zhen-Yi Zhang, Mohamedally Kurmoo, Zier Yan, Quan-Qin Zhao, Christine M. Aikens, Chen-Ho Tung, Di Sun. Different Silver Nanoparticles in One Crystal: Ag210(iPrPhS)71(Ph3P)5Cl and Ag211(iPrPhS)71(Ph3P)6Cl, Angewandte Chemie, 2019, vol. 58, iss. 1, pp 195-199, DOI: 10.1002/anie.201810772